A RECORD OF HOLOCENE CLIMATE CHANGE FROM THE SUNDA SHELF, SOUTH CHINA SEA

by

Anna Lee Woodson

November, 2014

Director of Thesis: Dr. Stephen J. Culver

Major Department: Geological Sciences

Variations in the East Asian Monsoon (EAM) control weather and regional climate conditions in the heavily populated, agriculturally dependent regions of eastern and southeast Asia. The South China Sea (SCS), especially the deep, northern SCS, has yielded many high-resolution Quaternary records of the EAM due to its high sedimentation rates and central location within the EAM system. The Sunda Shelf, a low-gradient, shallow region in the southwestern semi-enclosed SCS, is characterized by thin (~1 m) Holocene deposits and thus has not been a target for paleoclimate reconstructions. However, flooded fluvial paleochannels on the Sunda Shelf contain thicker, muddy Holocene sediments. Herein we test the hypothesis that the sediment fill of fluvial paleochannels contains a record of Holocene paleoclimate.

Two piston cores were collected in fluvial paleochannels ~80 km offshore of Bintulu, Sarawak, Malaysia. Core D45, collected on the edge of a v-shaped paleochannel, exhibits ~7200 years of sediment accumulation, whereas core D42, retrieved in a shallower paleochannel to the west, yielded a shorter (~3,000 year) but higher resolution record. Mg/Ca ratios of *Globigerinoides ruber* and *Globigerinoides sacculifer*, in combination with the stable oxygen isotopic composition of *G. ruber*, allow for the estimation of sea surface temperature (SST), the

stable oxygen isotopic composition of seawater ($\delta^{18}O_{sw}$), and salinity. Furthermore, the stable carbon isotopic composition of *G. ruber* illuminates trends in nutrient input and continental runoff.

Based on decreased salinity estimates, a high sedimentation rate (~0.064 cm/yr), and low $\delta^{13}C$ values, core D45 records an interval of increased rainfall and continental runoff from 6–4 ka, in keeping with nearby speleothem and continental pollen records. Additionally, this core records coeval reduced SST values, a trend not recognized in regional deep-sea records, suggesting a strong terrestrial runoff effect on the sedimentary record. The Medieval Climate Anomaly and Little Ice Age are also tentatively recognized in SST data. Core D42 shows similar trends in data for the late Holocene, confirming that flooded fluvial paleovalleys can provide Holocene paleoclimatic records on continental shelves characterized by generally low sediment accumulation rates.

A RECORD OF HOLOCENE CLIMATE CHANGE FROM THE SUNDA SHELF, SOUTH CHINA SEA

A Thesis

Presented to the Faculty of the Department of Geological Sciences

East Carolina University

In Partial Fulfillment of the Requirements for the Degree

Master of Science in Geological Sciences

by

Anna Lee Woodson

November, 2014

A RECORD OF HOLOCENE CLIMATE CHANGE FROM THE SUNDA SHELF, SOUTH CHINA SEA

by

Anna Lee Woodson

APPROVED BY:

DIRECTOR OF THESIS:_____
Stephen J. Culver, PhD, DSc.

COMMITTEE MEMBER: _____
Eduardo Leorri, PhD

COMMITTEE MEMBER: _____
David J. Mallinson, PhD

EXTERNAL COMMITTEE MEMBER: _____
Peter R. Parham, PhD

CHAIR OF THE DEPARTMENT
OF GEOLOGICAL SCIENCES: _____
Stephen J. Culver, PhD, DSc.

DEAN OF THE
GRADUATE SCHOOL: _____
Paul J. Gemperline, PhD

ACKNOWLEDGMENTS

Many thanks to Steve Culver, Edu Leorri, Dave Mallinson, and Pete Parham for their patience, encouragement, and guidance. This process would have been significantly less enjoyable without the comradery of my fellow graduate students. Thank you to Ray Tichenor, Caitlin Lauback, Alisha Ellis, and Hanna Thornberg for supporting me in the beginning, and to Kelli Moran, Jess Kegel, Devon Reed, Nick Zaremba, and Robbie Broda for helping me to the finish line. Additionally, I would also like to thank C.J. Whitley, Chris Bender, Eric Tappa, Kelly Gibson, Bob Thunell, Noor Shazili, Vijay Vijayan, Rob Howard, John Woods, and Jim Watson for technical support during various stages. NSF Grant OISE-1157222 provided financial support for this project. Thanks to Don Barber, Julie Griffin, and Erin Lynch for their unwavering friendship, for encouraging me to pursue geology at Bryn Mawr, and for consistently reminding me how fortunate I am to have discovered a field and a community that I love. I am eternally grateful to my parents for their unwavering confidence in me.

TABLE OF CONTENTS

LIST OF TABLES

LIST OF FIGURES

INTRODUCTION

Monsoons are the principal driver of weather and climate in Asia (Fong and Wang, 2001) and are controlled by differential heating between continents and oceans (Prell and Kutzbach, 1987; An et al., 1991). The East Asian Monsoon (EAM) influences wind patterns, precipitation, sea circulation, continental runoff, and nutrient transport (Cheng et al., 2005) from north China to areas surrounding the South China Sea (SCS) (Huang et al., 1997). Changes in EAM strength and duration can cause severe droughts or floods in these heavily populated regions (Webster et al., 1998). Thus, the EAM has the potential to affect agricultural productivity, which is of great economic importance to southeast Asian countries.

The EAM can be divided into two annual events: the summer and winter monsoons (An et al., 1991; Yoshino, 1971). From October to March, the East Asian Winter Monsoon (EAWM) drives cold, dry winds from the northeast; from May to September, the East Asian Summer Monsoon (EASM) drives southwesterly winds, bringing moist, tropical air to the region (Ding, 1994). These weather patterns result in seasonal temperature, salinity, and circulation fluctuations in the SCS (Wyrtki, 1961). In winter, the cold Chinese Coastal Waters are driven into the northern SCS, resulting in a north-south temperature gradient. During the EASM, warm Indian Ocean surface waters flow into the southern SCS, driven by southwesterly winds (Huang et al., 1997).

The deep, northern South China Sea (Figure 1) has been the focus of many Quaternary paleoclimatological studies because of its central location within the EAM system (e.g., Sarnthein et al., 1994; Wang et al., 1999) and its high sedimentation rates (2.5–7.1 cm/kyr during the Holocene) compared with the open ocean (Wang and Wang, 1990; Thunell et al., 1992; Wang et al., 1992; Miao et al., 1994). The Sunda Shelf occupies the southwestern, semi-

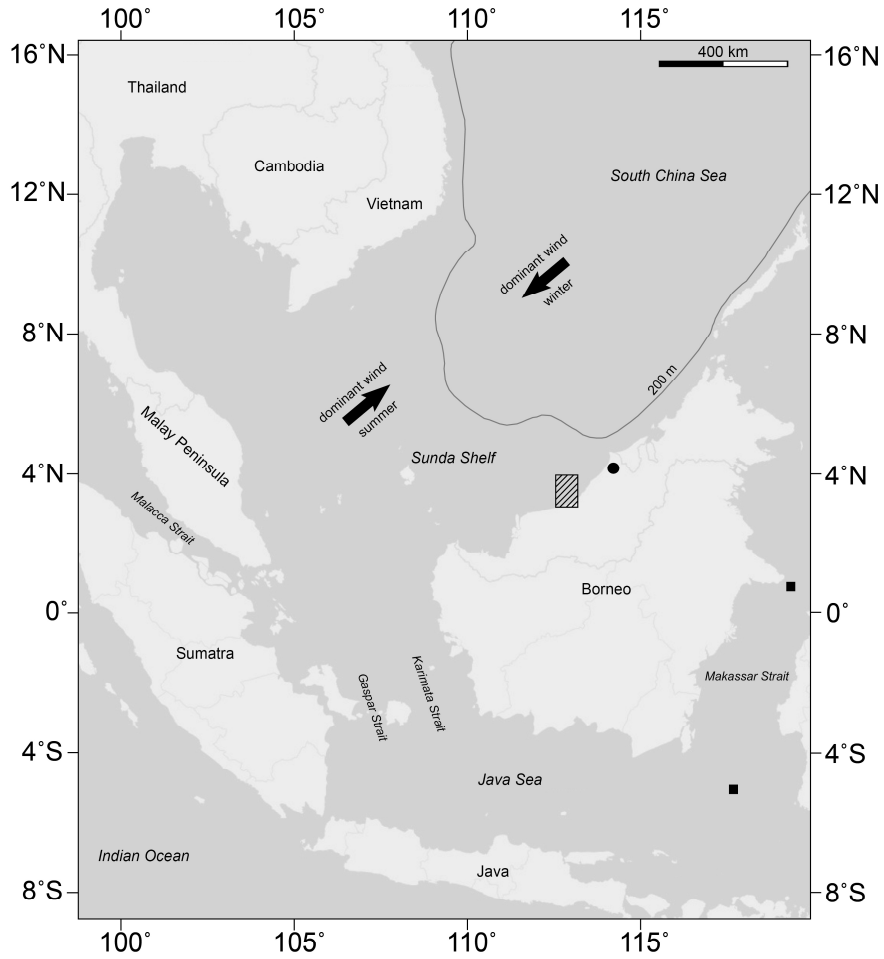

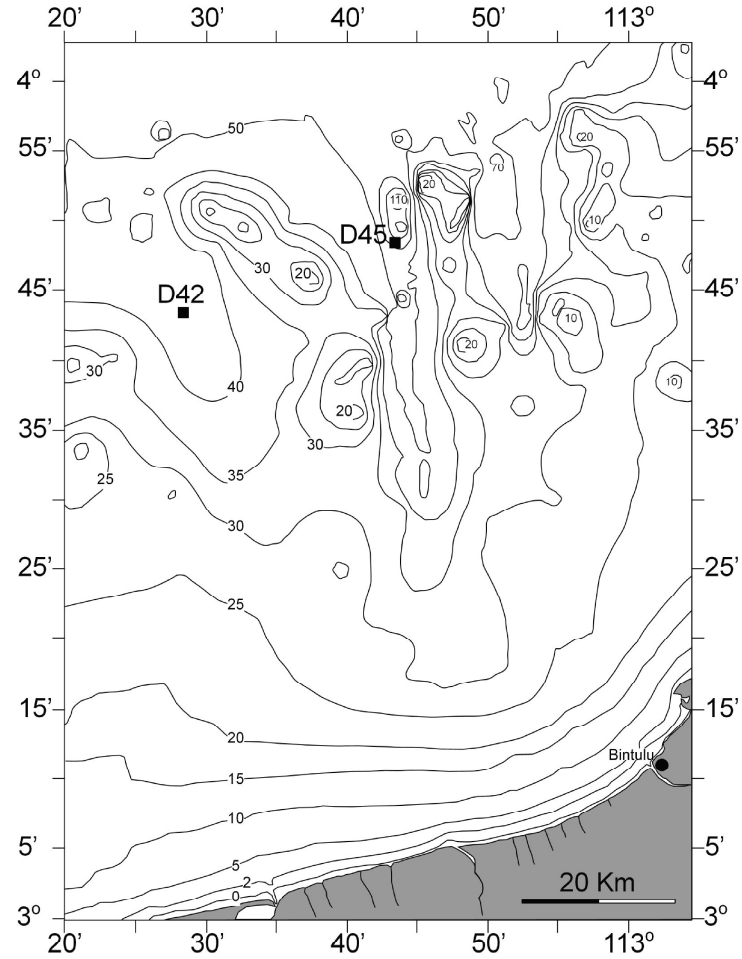

Figure 1 (left). A map of the Sunda Shelf and surrounding region. Black squares indicate locations of cores studied by Newton et al. (2006, 2011). The black circle marks Gunung Buda National Park, where Partin et al. (2007) measured stalagmite $\delta^{18}O$. The hashed rectangle indicates the area shown in Figure 2.

Figure 2 (right). Bathymetric map of the study area. Contours (m) were generated based on data from chart MAL 751, published December 31, 1993 by the Royal Malaysian Navy. Black squares indicate core locations.

enclosed South China Sea, providing the only connection to the Indian Ocean (through the Malacca Strait) and Java Sea (through the Gaspar and Karimata Straits). The shelf is bounded by the Malay Peninsula, the southern Indo-China peninsula, Sumatra, Borneo, and Java. It is extremely low-gradient (1:9,000), approximately 800 km in width, and averages ~70 m deep (Hanebuth and Stattegger, 2003). Average salinity on the Sunda Shelf is ~33 (Zweng et al., 2013), although salinity values near the outflows of the major rivers draining Borneo can be much lower at the end of the rainy season (Wyrtki, 1961). Sea surface temperatures range from approximately 26.5–28 °C in during the NE monsoon (winter) to 28–29.5°C during the SW monsoon (summer) (Locarnini et al., 2013).

The southern SCS, specifically the shallow, low gradient Sunda Shelf (Figure 1) has yet to yield a Holocene monsoon record due to its very thin sedimentary cover (Hanebuth et al., 2002, 2011; Hanebuth and Stattegger, 2003; Wong et al., 2003; Darmadi et al., 2007). However, many, now flooded fluvial valleys, incised during the lower sea-level conditions of the Last Glacial Maximum (LGM), contain a longer sedimentary record (Hanebuth et al., 2011). In this study, I 1) investigate whether Holocene sediment that has accumulated in two roughly southeast-northwest trending fluvial paleochannels off the coast of Bintulu, Sarawak, Malaysia (Figure 2) contains an archive of Holocene climate change and, 2) document variations in strength of the EAM over the past approximately 7,200 years.

BACKGROUND

Planktonic Foraminifera as Climate Proxies

Planktonic foraminifera, specifically shallow-dwelling species *Globigerinoides ruber* (D'Orbigny) and *Globigerinoides sacculifer* (Brady), are useful proxies of climate change because they record changes in seawater chemistry when they precipitate their tests. *G. ruber* is the ideal species for sea surface temperature (SST) and salinity reconstruction because it records conditions in the top ~30 m of the water column (Fairbanks et al., 1980, 1982; Mulitza et al., 1997). *G. sacculifer*, calcifying at ~25–40 m depth (Farmer et al., 2007), is also a good indicator of shallow ocean water properties. Based on a sediment trap study, *G. sacculifer* displays no seasonal calcification bias and is present throughout the year in the SCS, while *G. ruber* is present in higher percentages during warmer months (Lin et al., 2004).

Mg/Ca as a Proxy for Ocean Temperature

The Mg/Ca ratio of foraminiferal calcite is a widely used proxy for ocean temperature (Elderfield and Ganssen, 2000; Lea et al., 2000; Nürnberg et al., 2000; de Garidel-thoron et al., 2005; Bohaty et al., 2012). Mg is incorporated into the calcite lattice, but at 2–3 orders of magnitude less than Ca (Morse and Bender, 1990). Increases in Mg content correspond with elevated seawater temperatures (Wefer et al., 1999). Because Mg and Ca have relatively long residence times in the ocean, Mg/Ca is a reliable temperature proxy. Secondary controls on Mg/Ca include pH, carbonate ion concentration, and salinity, but most studies indicate that the temperature effect is dominant (Nürnberg et al., 1996; Lea et al., 1999; Russel et al., 2004; Hönisch et al., 2013).

Inter-species variability of Mg/Ca is high (Morse and Bender, 1990), so Mg/Ca-temperature relationships must be determined by robust calibration studies using core-top samples, sediment traps, or cultured foraminifera (e.g., Anand et al., 2003; Elderfield and Ganssen, 2000; Elderfield et al., 2006; Nürnberg et al., 1996; Regenberg et al., 2009). Error ranges for Mg/Ca to temperature conversions are typically 0.5 to 1.0°C (Elderfield and Ganssen, 2000; Lea et al., 2000; Hastings et al., 2001; Dekens et al., 2002; Anand et al., 2003).

Stable O and C Isotopes as Proxies for Paleoenvironment

Oxygen isotopic data from tests of planktonic foraminifera provide information on past temperature and salinity conditions of surface water (Cheng et al., 2005). Enriched $\delta^{18}O$ values represent a decrease in freshwater input from land or from direct rainfall (i.e., decreased precipitation/evaporation), while depleted values suggest the opposite (Rashid et al., 2011). $\delta^{18}O$ of foraminiferal ($\delta^{18}O_c$) tests can be paired with Mg/Ca-based temperature estimates to produce seawater $\delta^{18}O$ ($\delta^{18}O_{sw}$), a proxy for sea surface salinity (SSS; e.g. Schmidt et al., 2006; Schmidt and Lynch-Stieglitz, 2011; Weldeab et al., 2007).

Additionally, nutrient availability and upwelling trends can be studied using stable carbon isotopes of planktonic foraminiferal tests. A decrease in $\delta^{13}C$ suggests an increase in nutrient concentrations and a decrease in oxygen availability (Mulitza et al., 1999). Additionally, because river water typically displays a more depleted $\delta^{13}C$ signature than seawater, a decrease in $\delta^{13}C$ may imply an increase in terrestrial runoff (Moyer and Grottoli, 2011).

Quaternary EAM Records

Many studies have reported a strengthened glacial EAWM and enhanced interglacial EASM based on proxies such as pollen and spores in SCS sediments (Sun et al., 1999), variations in terrigenous sediment grain size, $\delta^{18}O$ and $\delta^{13}C$ of planktonic foraminifera, alkenones (Wang et al., 1999), and radiolarian abundance (Wang and Abelmann, 2002). Additional trends have been observed throughout the Quaternary. Huang et al. (1997) studied sediment cores from Toushe Lake in Taiwan, noting high sedimentation rates, rain-related clay layers, and abundant thermophytes during the Holocene and suggesting a strengthened EASM relative to the LGM for this time period. Based on decreases in winter sea surface temperature and increases in productivity gleaned from SCS sediments, they also proposed a strong EAWM during the LGM, followed by a weakening from 12 to 10 kya. A similar paleoclimatic record has been reported in studies of Chinese loess-paleosol sequences (Maher et al., 1994; Xiao et al., 1995).

Numerous studies have been conducted on the Holocene EAM throughout the SCS. Miao et al. (1994) generated a 25,000 year long SST record in the eastern deep SCS and Sulu Sea from cores collected in 500–4000 m deep water. Their SST reconstruction was based on a planktonic foraminiferal transfer function developed by Thompson (1981). Additionally, they measured oxygen isotopes of *G. sacculifer*. Cores from <3000 m depth yielded an average Holocene summer SST of 29°C, 1–2 degrees warmer than during the LGM.

Northern SCS EAM studies have included both deep-sea and coastal paleoclimate reconstructions. High-resolution $\delta^{18}O$ and Sr/Ca records of *Porites lutea* corals from the northern coast of the SCS reveal generally decreasing SST and $\delta^{18}O_{sw}$ from ~6.8 to 1.5 ka, with temperatures ~0.7°C cooler than present ~1.5 ka (Yu et al., 2005).

Kong et al. (2014) reconstructed SST over the past ~8000 years using the long-chain alkenone unsaturation index from two cores, one from the deep, northern SCS and a second from a shallow core in the Pearl River Estuary. Their cores recorded different SST signals. The shallow, coastal data showed stable, warm temperatures during the mid-Holocene, followed by a cooling trend until the present. The deeper SCS record suggested warming from 8 to 3.5 ka, followed by relatively stable and warm temperature. Kong et al. (2014) suggested the difference between coastal and deep-sea records was due to a stronger EAWM since ~7 ka contributing to coastal cooling. Other alkenone-based SST studies in the northern SCS (Huang et al., 1997; Wang et al., 1999) and southern deep SCS (Kienast et al., 2001) also revealed warm SST in the mid- to late Holocene.

High-resolution SST records have also been produced in the southern deep SCS using foraminiferal proxies such as census counts (Steinke et al, 2001), as well as Mg/Ca and oxygen isotopes (Steinke et al., 2006, 2010). Steinke et al. (2006) estimated SST for a deep-sea core using the Hastings et al. (2001) Mg/Ca-temperature relationship for *G. ruber*. Additionally, in combination with their SST estimates, $\delta^{18}O$ of *G. ruber* provided a $\delta^{18}O_{sw}$ record (using the Bemis et al., 1998 equation). Using the same core, Steinke et al. (2010) compared the *G. ruber* data with $\delta^{18}O$ and Mg/Ca of *Pulleniatina obliquiloculata* (a thermocline-dwelling planktonic species), as well as alkenone-based temperature estimates, in order to study the vertical structure of the southern deep SCS. These comparisons served as a proxy for EAWM wind strength and surface water mixing. Based on the Steinke et al. (2010) results, the EAWM was weakest from 6.5–2.5 ka.

Additional Holocene EAM studies (Newton et al., 2006, 2011) using Mg/Ca and $\delta^{18}O$ of *G. ruber* were conducted in the Makassar Strait, on the southeastern coast of Borneo (Figure 1).

These high-resolution reconstructions recorded maximum SST and SSS 850–700 years ago (the Medieval Warm Period) and minimum SST and SSS 300–100 years ago (the Little Ice Age).

Holocene EAM records from landmasses surrounding the SCS largely comprise speleothem oxygen isotope records, a proxy for monsoon rainfall. Data from Dongge (southern China; Dykoski et al., 2005; Wang et al., 2005), Heshong (southwest China; Hu et al., 2008), Wanxiang (central China; Zhang et al., 2008), and Sanbao caves (central China; Dong et al., 2010) suggest EASM weakening during the Holocene related to decreasing summer insolation. More recent records by Selvaraj et al. (northeastern Taiwan; 2012) and Zhao et al. (a synthesis of marine and terrestrial data from the western Pacific and Indian Oceans; 2013) suggest that EASM may have strengthened in the late Holocene.

Partin and others (2007) provided a U–Th dated $\delta^{18}O$ record from the island of Borneo. They sampled three stalagmites from Gunung Buda National Park (Figure 1) in northwestern Borneo, interpreting a $\delta^{18}O$ decrease at ~5 ka as an increase in mid-Holocene rainfall.

METHODS

Piston cores D42 (3° 43.575’ N, 112° 28.198’ E, 3.88 m long, 52.33 m water depth) and D45 (3° 48.611’ N, 112° 43.632’ E, 2.68 m long, 62.51 m water depth) were collected in the sedimentary fill of flooded fluvial paleochannels on the Sunda Shelf approximately 80 km northwest of Bintulu, Sarawak, Malaysia by the Department of Minerals and Geosciences Malaysia in July of 2008 (Figure 2; Appendix A). In January of 2013, these cores were subsampled at contiguous, 2-cm intervals.

Between 5 and 48 g of each dry sample were lightly crushed with a pestle and soaked in distilled water, 100–150 mg of sodium hydroxide (NaOH) and approximately 150 mg of sodium metaphosphate ($(NaPO_3)_x \bullet Na_2O$) for 12–24 hours to aid in disaggregation. Samples were then washed over 63- and 125-µm sieves to remove mud and isolate larger foraminifera. The 63–125 µm and >125 µm fractions were dried in an oven at 60°C. Tests of foraminifera were picked from the >125 µm fraction with a paintbrush and distilled water. Species identifications were verified with collections housed at the Smithsonian Institution, Washington, DC.

Mg/Ca

Between 200 and 450 micrograms (11–34 tests) of *G. ruber* and *G. sacculifer* were used for Mg/Ca analysis. The samples were cleaned following standard procedures (Boyle, 1981; Appendix B), excluding the reductive step, to remove clay and organic matter. Mg and Ca values were measured on a Jobin Yvon Ultima inductively coupled plasma atomic emission spectrophotometer (ICP-AES) at the University of South Carolina.

Sea surface temperatures were estimated using the warm water, multi-species Mg/Ca-temperature relationship developed by Regenberg et al. (2009):

$$Mg/Ca = 0.22e^{0.113T}.$$

The average error for this calculation is ±0.26 °C.

Stable Oxygen and Carbon Isotopes

Five to six *G. ruber* tests per sample were used for stable oxygen and carbon isotopic analysis. Samples were analyzed on a VG Optima stable isotope ratio mass spectrometer (IRMS) at the University of South Carolina. $\delta^{18}O_c$ results were reported relative to the Vienna Pee Dee Belemnite standard. Long-term standard reproducibility is ±0.07‰ for $\delta^{18}O$ and ±0.04‰ for $\delta^{13}C$.

Previously calculated temperatures and $\delta^{18}O_c$ values were converted to $\delta^{18}O_{sw}$ with the Bemis et al. (1998) paleotemperature equation for *G. ruber* (standard error = 0.5°C)

$$T(°C) = 14.9 - 4.80(\delta^{18}O_c - \delta^{18}O_{sw}).$$

Salinities were calculated using the modern relationship between $\delta^{18}O_{sw}$ and salinity for the Western Pacific (Morimoto et al., 2002)

$$\delta^{18}O_{sw}(SMOW) = 0.42S - 14.3.$$

Radiocarbon Age Estimates

Accelerator mass spectrometer (AMS) radiocarbon dating of 4.0–14.5 mg of the benthic foraminifer *Cavarotalia annectens* provided a geochronological framework. Eight samples from D42 and 21 samples from D45 were submitted to NOSAMS (the National Ocean Sciences Accelerator Mass Spectrometry Facility) or Beta Analytic for AMS ^{14}C age analysis. The R/Bchron package (Haslett and Parnell, 2008; R Development Core Team, 2011) was used to calibrate radiocarbon age estimates (Marine09 calibration curve; Reimer et al., 2009; Appendix

C) and generate age-depth models. Calibrated ages were compared with age estimates produced by Calib 7.0 using the Marine13 calibration curve (Reimer et al., 2013; Table 1) and no significant differences were identified.

RESULTS

Geochronology

Twenty-nine AMS radiocarbon age estimates of the benthic foraminifer *Cavarotalia annectens* provide chronologic control for cores D42 and D45 (Table 1). Twenty-one age estimates from D45 ranged from 6650–930 ^{14}C yr BP (7318–499 cal yr BP). Three samples (3890, 2820, and 3050 ^{14}C yr BP at 107 cm, 91 cm, and 79 cm, respectively) were excluded from the age-depth model (Figure 3; Appendix D) because these ages were older than those preceding them stratigraphically and were considered to be the result of reworking.

Calibrated 2σ ages for D42 range from 3353 to 639 cal yr BP. One sample, from 386–388 cm deep in the core (the lowest sample), returned an age estimate of 340 ± 30 ^{14}C yr BP (50–10 cal yr BP). We hypothesize that modern sediment was unintentionally sampled at the base of the core (corer bounce on the seabed) during the process of core recovery. This sample has been eliminated from the age-depth model (Figure 4; Appendix E). Three samples from 198–358 cm depth returned ages of ~3100–3500 cal yr BP. This suggests possible mixing of the core for this interval. Consequently, remaining analyses were performed on only the top section of the core (0–150 cm, ~2.2 ka to the present).

Sedimentation Rates

Four phases of sedimentation are reflected in the D45 age-depth model (Figure 3). From ~7.2–5.5 ka, sedimentation rates were fairly slow, at ~0.022 cm/yr (~90 yr/sample resolution). After ~5.5 ka, sedimentation rates increased to ~0.064 cm/yr (~30 yr/sample resolution) until ~4.0 ka. Deposition was relatively slow (~0.013 cm/yr; ~155 yr/sample resolution) from ~4.0–2.2 ka. Data from this latter section of the core should be considered cautiously since each

Table 1. Radiocarbon age estimates. Age ranges reported here were calibrated using the Reimer et al. (2013) dataset.

Sample ID	Depth in core (m)	Age (^{14}C yr BP)	2σ Age Range (cal yr BP)	
D042_8-10	-0.09	1130 ± 30	639	807
D42_24-26	-0.25	1820 ± 25	1308	1508
D42_56-58	-0.57	1880 ± 25	1357	1559
D42_110-112	-1.11	2350 ± 25	1906	2128
D42_198-200	-1.99	3450 ± 35	3234	3485
D042_276-278	-2.77	3330 ± 30	3106	3350
D42_356-358	-3.57	3340 ± 25	3131	3353
D042_386-388	-3.87	340 ± 30	10	50
D045_10-12	-0.11	930 ± 30	499	635
D45_16-18	-0.17	1110 ± 25	635	776
D45_24-26	-0.25	1010 ± 30	535	680
D45_34-36	-0.35	1580 ± 25	1076	1267
D45_48-50	-0.49	1900 ± 25	1378	1590
D45_60-62	-0.61	2070 ± 30	1566	1807
D45_74-76	-0.75	2260 ± 25	1808	2022
D45_78-80	-0.79	3050 ± 30	2749	2970
D45_90-92	-0.91	2820 ± 25	2485	2726
D45_98-100	-0.99	2540 ± 20	2145	2334
D45_106-108	-1.07	3890 ± 25	3807	4056
D45_112-114	-1.13	3470 ± 35	3263	3520
D45_122-124	-1.23	4100 ± 35	4068	4368
D45_132-134	-1.33	4310 ± 30	4369	4623
D45_148-150	-1.49	4410 ± 30	4502	4787
D45_162-164	-1.63	4600 ± 30	4778	4990
D45_182-184	-1.83	4820 ± 30	5022	5290
D45_198-200	-1.99	5010 ± 30	5295	5520
D45_214-216	-2.15	5180 ± 40	5463	5687
D45_232-234	-2.33	5950 ± 25	6294	6492
D045_248-250	-2.49	6650 ± 30	7132	7318

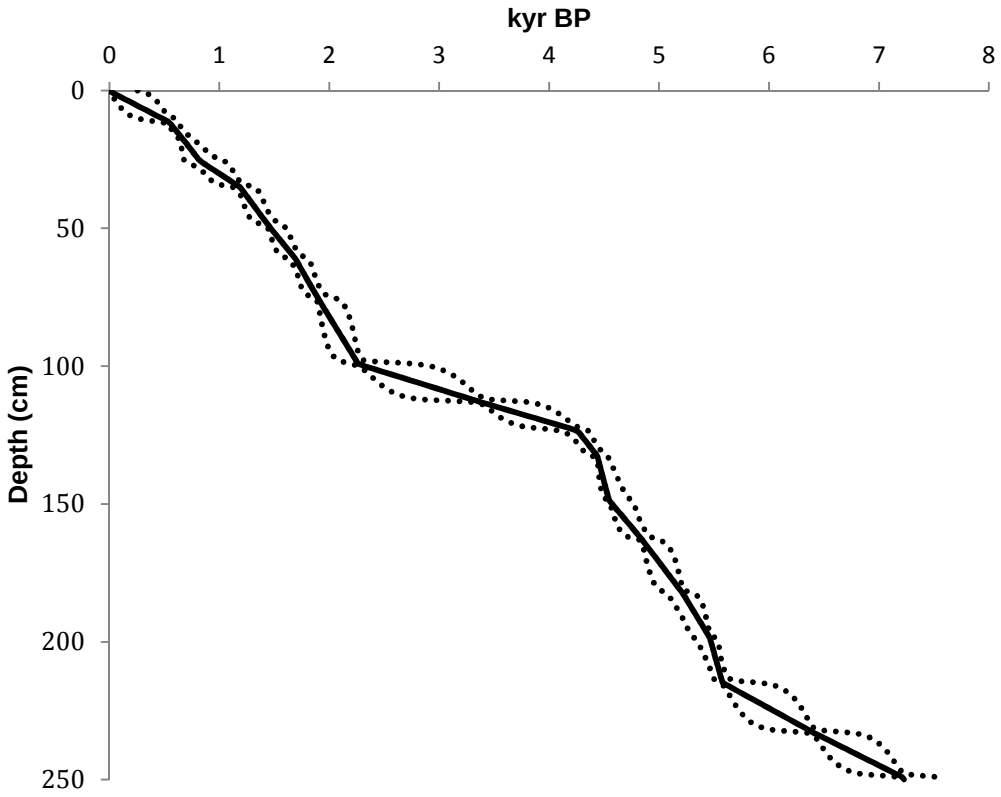

Figure 3. Age-depth model for core D45. Dotted lines indicate the 95% confidence interval.

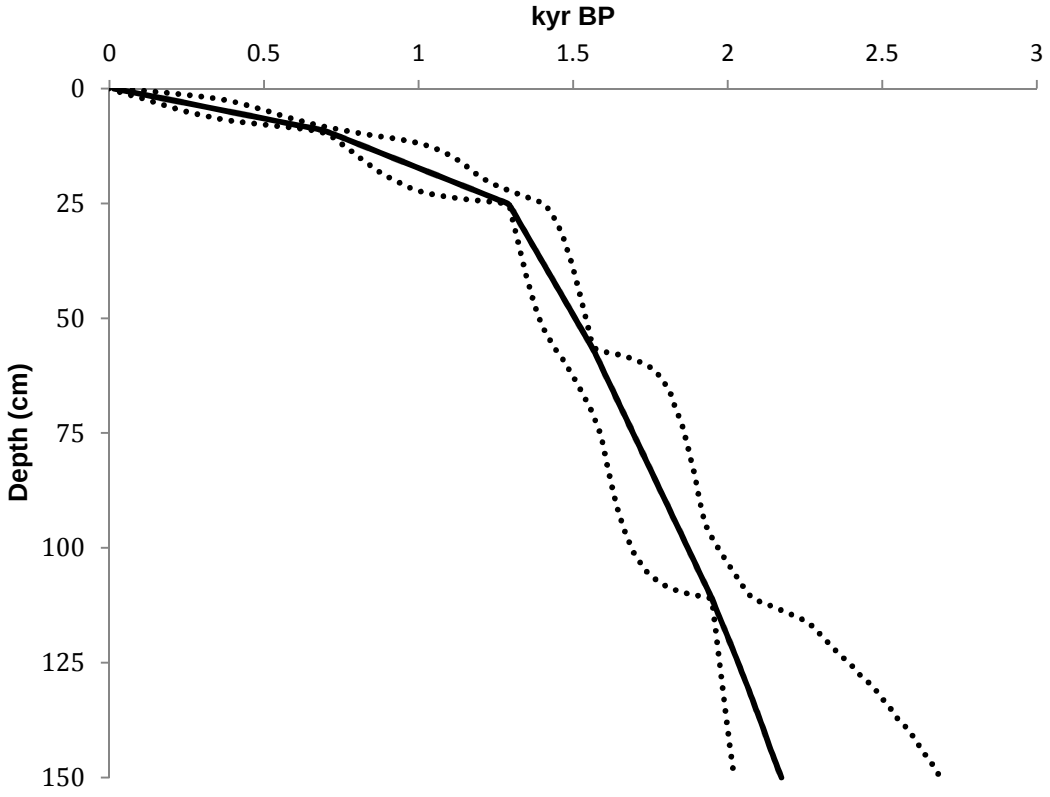

Figure 4. Age-depth model for core D42. Dotted lines indicate the 95% confidence interval.

sample represents a comparatively long time interval. After ~2.2 ka, sedimentation rates increased to ~0.044 cm/yr (~45 yr/sample resolution). Based on the D42 age-depth model (Figure 4), there is a change in sedimentation rate at ~1.3 ka from approximately 0.14 cm/yr (~14 yr/sample resolution) to ~0.02 cm/yr (~100 yr/sample resolution).

Sedimentology

Sediments from D42 and D45 comprise gray mud. Sand-sized particles are composed of whole and fragmented biogenic material including foraminifera, gastropods, bivalves, sponge spicules, etc. The bottom 18 cm of D45 (250–268 cm deep; not shown on Figure 5) are barren of

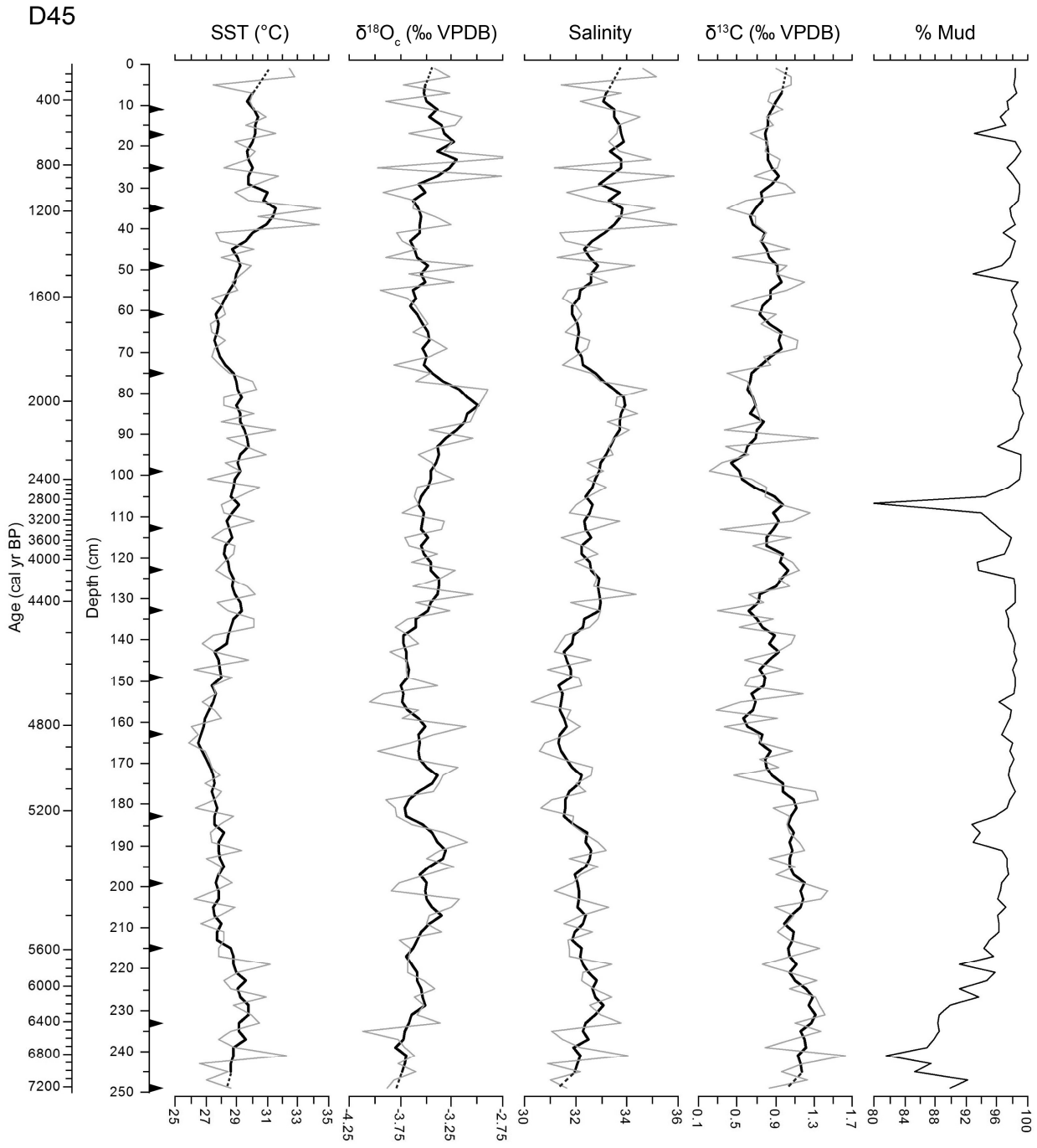

Figure 5. Sea-surface temperature, salinity, grain size, and stable isotopic data for core D45. Time series are plotted in gray and five-point moving averages are shown in black. Since the smoothing process eliminates two data points at both the top and base of the core, estimated trends have been marked by with dashed lines. Black triangles indicate the location of radiocarbon age estimates. Data used to construct this figure are located in Appendices F, H, and J.

shell material (comprise only mud with some fine plant fragments). Percent mud values for D45 range from 80–99% (Figure 5). There is a shell-rich interval from 220–250 cm (peaking at 240–242 cm), but mud content remains above 80%. A minimum percent mud value of 80% from 107–109 cm (~2.9 ka) marks a layer with significantly more abundant shell material than is contained in surrounding samples.

D42 comprises slightly finer, more homogeneous sediment than D45, with percent mud values ranging from 95 to 99% (Figure 6). Mud content increases up-core to ~68 cm depth (~1.65 ka). Percent mud becomes more variable in the upper section of the core, with slightly coarser, shelly intervals from 36–38 cm (~1.4 ka) and 18–20 cm (~1.0 ka).

Sea Surface Temperature Records

Sea surface temperatures reconstructed from Mg/Ca of *Globigerinoides ruber* and *Globigerinoides sacculifer* in D45 (Figure 5) range from 25.9–34.5°C, with an average value of 28.7°C. Application of a five-point moving average to reduce the noise of the data set (Steinke et al., 2014) indicates that there is a warming trend from ~7.2–6.2 ka, at which point SST begins to decrease until ~4.9 ka. This was followed by a warming event from ~4.9–4.5 ka. Data from the period ~4.4–2.2 ka must be interpreted cautiously due to the slow sedimentation rate and resulting poor resolution, but temperatures appear to be relatively stable. Temperatures decrease from ~2.0–1.8 ka, then increase until ~0.04 ka with a peak from ~1.3–1.0 ka.

Reconstructed temperatures in D42 (Figure 6) range from 26.3–32.9°C with an average value of 28.7°C, comparable to D45. A five-point moving average of this record indicates generally stable temperatures from ~2.17 ka to ~1.4 ka with a possible short peak from ~1.8–1.7 ka. Temperature rose slightly from ~1.4–0.1 ka.

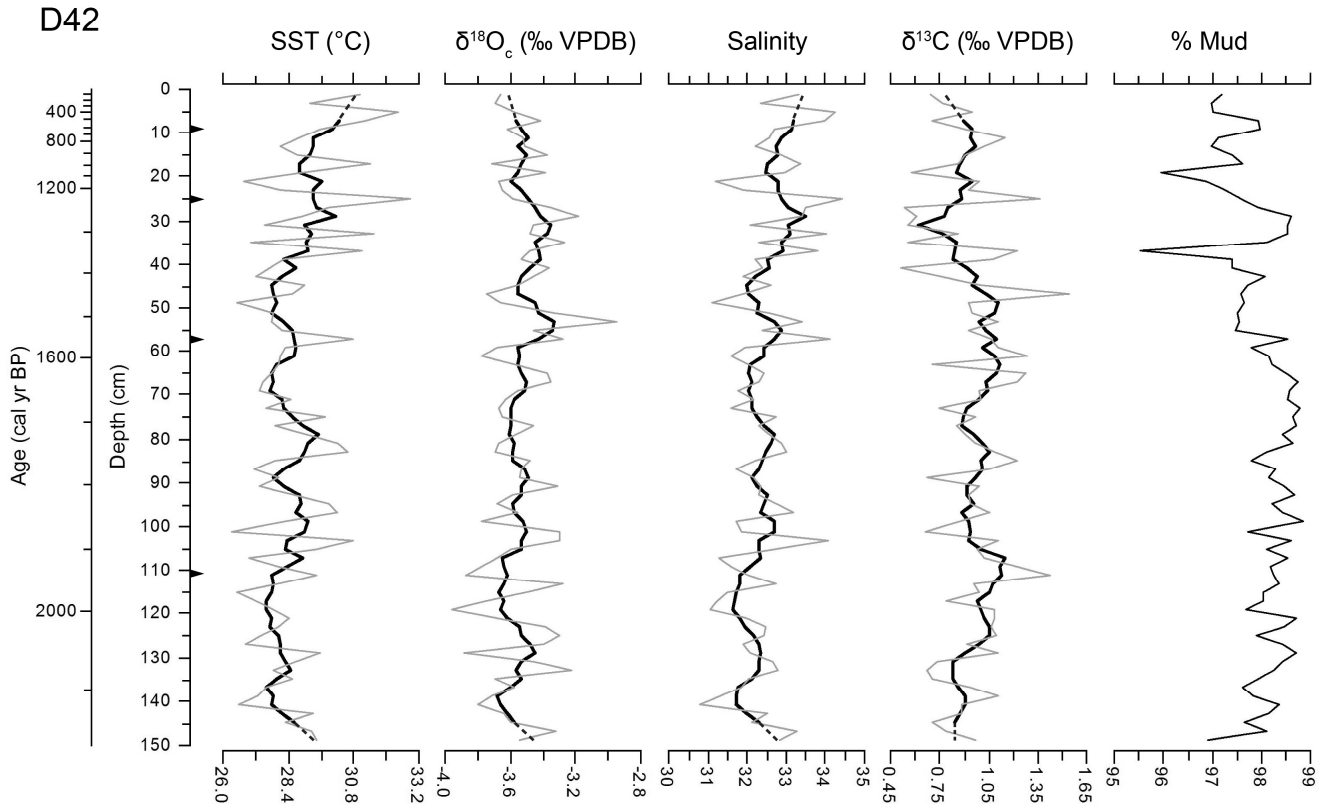

Figure 6. Sea-surface temperature, salinity, grain size, and stable isotopic data for core D42. Time series are plotted in gray and five-point moving averages are shown in black. Since the smoothing process eliminates two data points at both the top and base of the core, estimated trends have been marked by with dashed lines. Black triangles indicate the location of radiocarbon age estimates. Data used to construct this figure are located in Appendices G, I, and K.

Salinity Records

D45 salinity values (Figure 5) range from 30.3 to 36.0 with an average of 32.5. Based on the smoothed curve, salinities mirror temperature trends, generally increasing from ~7.2–6.2 ka, then decreasing slightly until ~4.6 ka. There is a rapid increase from ~4.6–4.4 ka. Following this peak, salinity remains stable until ~2.8 ka, then increases to ~2.0 ka. Salinity decreases from ~2.0–1.7 ka and then increases to ~1.2 ka. The curve is stable from ~1.2–0.4 ka, but appears to increase until ~0.04 ka.

D42 salinities (Figure 6) range from 30.8 to 34.4 with an average of 32.5. As for D45, reconstructed salinities mirror temperature trends (stable from ~2.17–1.4 ka, then slightly increasing from ~1.4–0.1 ka).

Stable Carbon Isotopic Records

D45 $\delta^{13}C$ values (Figure 5) range from 0.22–1.63‰ (average = 0.90‰). $\delta^{13}C$ is stable or slightly increases from ~7.2–6.3 ka, then decreases to ~4.8 ka. There is an increasing trend until ~4.5 ka. $\delta^{13}C$ is generally level (with oscillations) until ~2.8 ka, then decreases until ~2.3 ka. From ~2.3 ka to ~40 years ago, $\delta^{13}C$ oscillates but increases slightly.

D42 $\delta^{13}C$ values (Figure 6) range from 0.52–1.54‰ with an average of 0.94‰. Based on the smoothed curve, $\delta^{13}C$ generally increases from ~2.2–1.9 ka, remains stable until ~1.7 ka, increases to ~1.5 ka, then decreases until ~1.3 ka. After this point, $\delta^{13}C$ increases to ~400 years ago and then decreases.

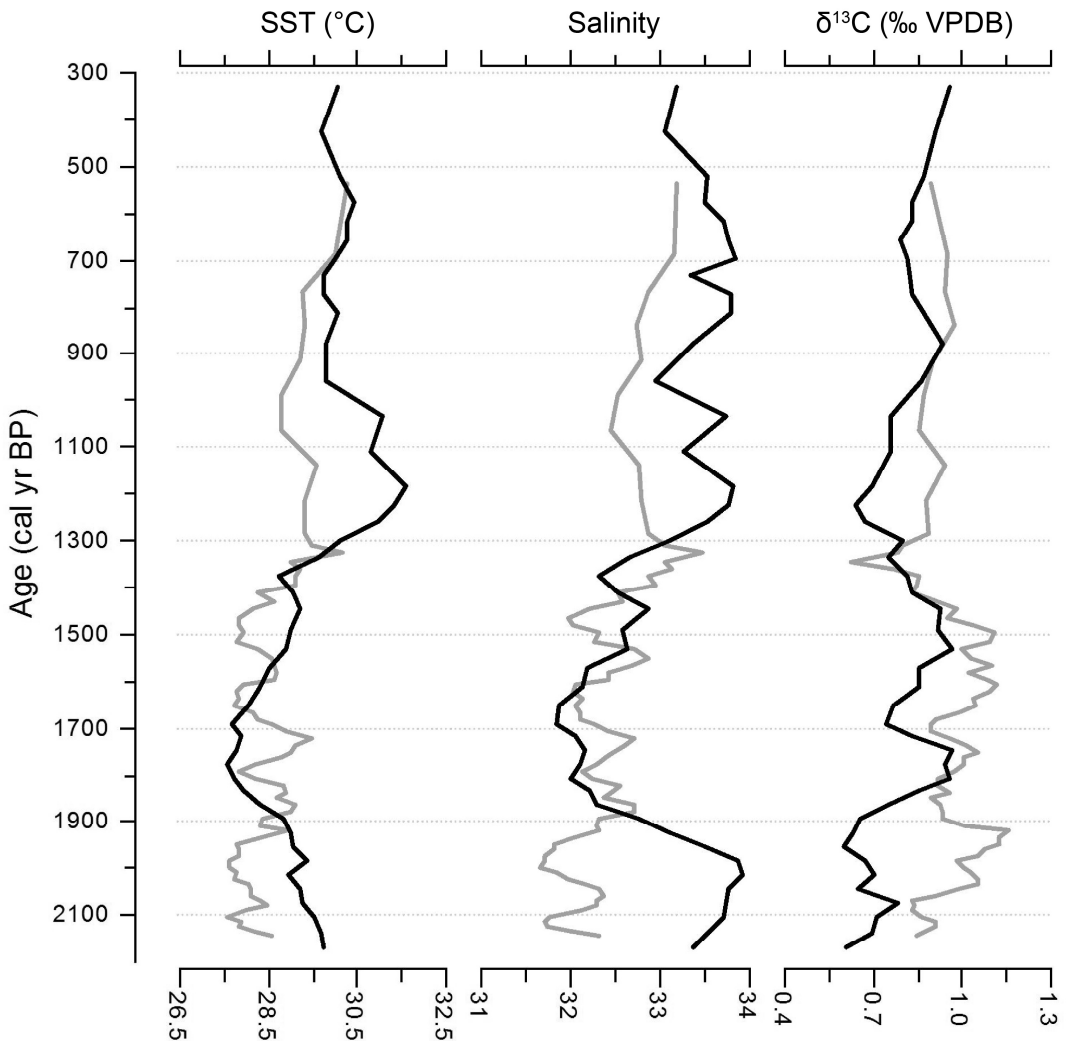

Figure 7. Five-point moving averages of sea surface temperature, salinity, and stable carbon isotopic data from cores D45 (black) and D42 (gray) for the last ~2.2 ka.

Core Comparison

A comparison of five-point moving averages of SST, salinity, and $\delta^{13}C$ from D45 and D42 for the last ~2.15 ka (Figure 7) reveals general agreement between the two records, especially during the period ~1.9–1.3 ka. From ~2.15–1.9 ka, the records diverge, most likely a result of the large uncertainty in the D42 age-depth model at this time. From ~1.3–0.3 ka, the records are also slightly offset, although differences are minimal when the reconstruction errors are considered. Age control in D42 is poor for this time interval (only one age estimate, at ~700 cal yr BP), however local differences (e.g., proximity to fluvial discharge) may also affect these signals.

DISCUSSION

SST Estimates

Compared to modern, instrument-measured conditions on the Sunda Shelf, reconstructed core top SST and salinity estimates are elevated. Core top (0–2cm) SSTs for D42 and D45, 31.0 and 32.4°C, respectively, are elevated at least 1–2°C above summer temperatures (28–29.5°C). D42 and D45 core top salinity values (33.3 and 34.6) are also slightly higher than the modern average on the shelf (33, but closer to 30 near river mouths). There are several possible explanations why SSTs and, therefore, salinities are elevated. Of these, the first is the most likely.

1. The Regenberg et al. (2009) Mg/Ca-temperature relationship utilized in this study may not be appropriate for Sunda Shelf foraminifera. In a study conducted by Rosenthal et al. (2003) in the Sulu Sea, SST estimates calculated based on a Pacific, open-ocean calibration were elevated relative to modern values. The authors suggested that because carbonate preservation was better in the shallow Sulu Sea than in the Pacific, and because high-Mg calcite is preferentially dissolved, their SST estimates were higher than expected. They suggested, therefore, that open ocean calibrations might not be appropriate for studies involving shelf foraminifera. The Regenberg et al. (2009) equation was selected because the calibration involved multiple shallow and thermocline dwelling species in warm water, but differences in test preservation may skew the reconstruction. However, the Regenberg et al. (2009) study stated that carbonate preservation in their samples was excellent “as indicated by the presence of aragonitic pteropod shells down to water depths of ≈3000m.”

2. High-Mg overgrowths may form in $CaCO_3$ supersaturated pore water, elevating measured Mg/Ca (Hertzberg and Schmidt, 2013). However, specimens in this study are small (<250 micrometers), delicate, and do not show evidence of overgrowth.
3. Including a reductive step (which removes Mn-oxide precipitates and Mn-rich carbonate coatings) in the cleaning process reduces Mg/Ca (Hertzberg and Schmidt, 2013). A difference in cleaning protocol between this study and the the Regenberg (2009) calibration study would result in additional SST calculation error. However, neither cleaning procedure involved a reductive step; foraminifera were washed with water and methanol and treated with hydrogen peroxide and a weak acid leach. Thus, this is not a possible explanation for the elevated values.
4. Foraminiferal tests that precipitate in high salinity environments (above 35.5) have elevated Mg/Ca values, which lead to high SST estimates (Hertzberg and Schmidt, 2013). This is not a contributing factor on the Sunda Shelf because of its extensive freshwater input.

Comparison with Regional Records

Due to changes in resolution related to sedimentation rate variability and the Holocene focus of this study, comparison with longer regional EAM records (e.g., Wang, 2000; Miao et al., 2004) is problematic. Additionally, the errors involved in the measurement of Mg/Ca and conversion to SST estimates, as well as the subsequent calculation of $\delta^{18}O_{sw}$ and salinity, overshadow some higher frequency fluctuations in these values throughout the Holocene. However, despite the potential limitations, longer-term salinity trends in core D45 mirror

changes in rainfall inferred from several stalagmite oxygen isotope records in Gunung Buda National Park, northwestern Borneo (Figure 1, D1; Partin et al., 2007).

Reconstructed salinity estimates in D45 decrease to a broad minimum ~6–4 ka (a trend also reflected in $\delta^{13}C$ values), the same time that the Borneo speleothems record a decrease in $\delta^{18}O$ values, indicating an increase in rainfall (Figure 8). The sedimentation rate of D45 was highest (~0.064 cm/yr) from ~5.5–4.0 ka, suggesting increased continental runoff. Following this wetter interval, both stalagmite $\delta^{18}O$ and D45 salinity values generally increase, suggesting a decrease in rainfall during the late Holocene. Partin et al. (2007) suggested that the Intertropical Convergence Zone (ITCZ) migrated southward during the mid-Holocene as a response to precessional forcing, crossing the equatorial Pacific and delivering more rainfall to the study area ~5 ka. D45 SST values are also coolest around 5 ka, a trend that is not evident in the deep SCS (e.g., Kienast et al., 2001) or Makassar Strait (Linsley et al., 2010) SST reconstructions (Figure 8). The shallow Sunda Shelf record is likely more sensitive than the deep SCS to temperature and salinity shifts influenced by changes in rainfall patterns and continental runoff.

In further support of a strong terrestrial runoff effect on the Sunda Shelf sedimentary record, trends in salinity observed in this study agree with Holocene rainfall conditions in mainland Southeast Asia. Using pollen records from 15 sites throughout the region, Chabangborn and Wohlfarth (2014) identified a dry period from 7–6.5 ka associated with warm temperatures. They also noted increased rainfall from 6.5–5 ka but their record did not include data more recent than 5 ka.

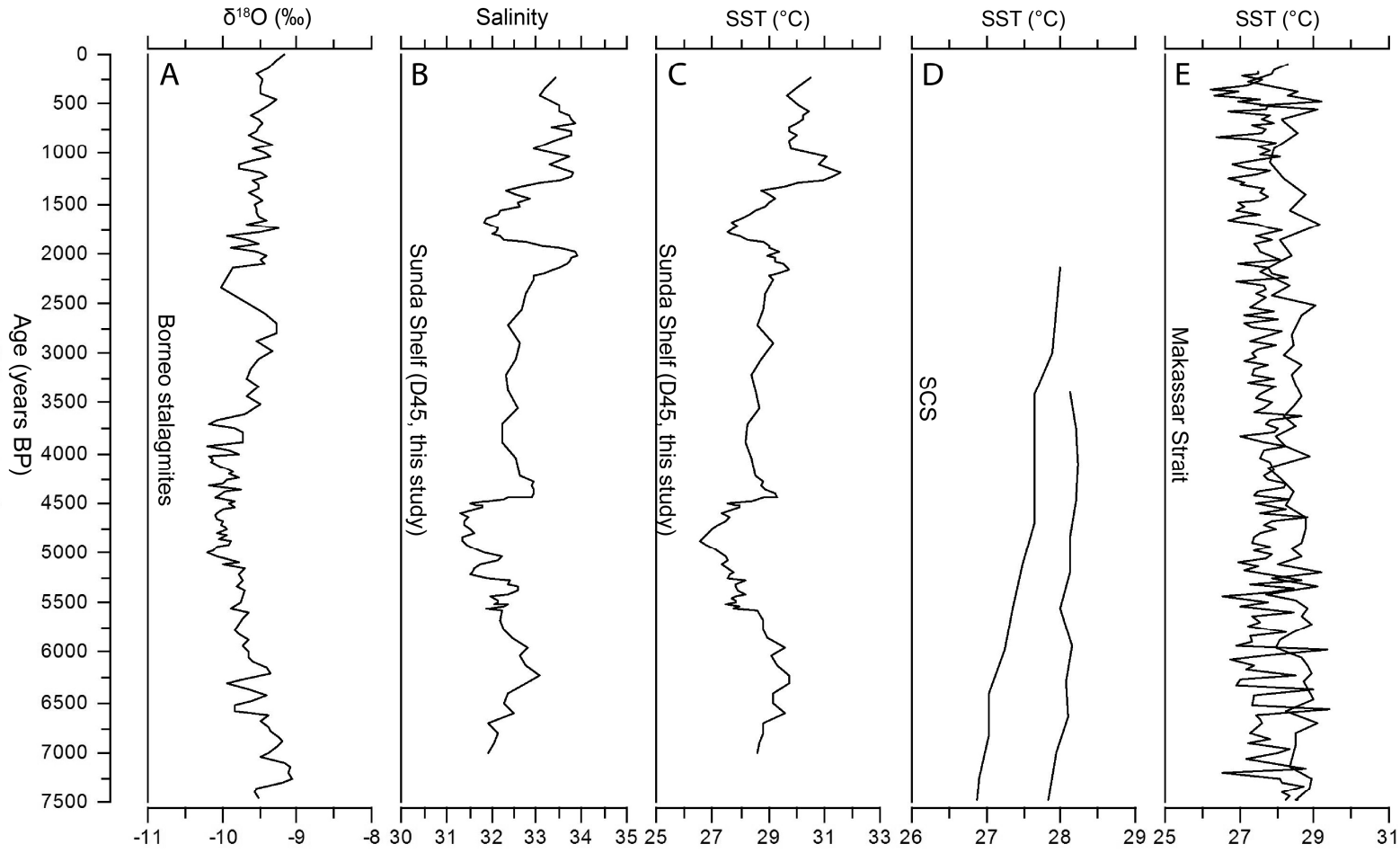

Figure 8. EAM proxy records: A, $\delta^{18}O$ of stalagmites from Gunung Buda National Park, Borneo (Partin et al., 2007); B, D45 salinity and C, SST estimates from the Sunda Shelf (this study); D, SST reconstructions from sediment cores in the deep SCS (Kienast et al., 2001) and E, Makassar Strait (Linsley et al., 2010).

Medieval Climate Anomaly and Little Ice Age

Based on the smoothed D42 and D45 SST records, geographically widespread climate events such as the Medieval Climate Anomaly (MCA) and Little Ice Age (LIA), previously documented in other regional paleoclimate studies (e.g., Newton et al., 2006, 2011; Rosenthal et al., 2013; Kong et al., 2014), may be recognizable in these sediments. Both cores exhibit a brief increase in SST centered on ~1.2 ka (more evident in D45), followed by a decrease approximately 400 years ago (Figure 7). However, these events are supported by very few (1–3) data points. Additionally, within error (~1°C), these low amplitude (~3–5°C and ~2–3°C for the MCA and LIA, repectively) excursions may not be significantly anomalous. Records of these climatic events could be further explored in cores from the Sunda Shelf with higher resolution sampling. This would necessitate the collection of a number of replicate cores to account for the low abundance of planktonic foraminifera on the mid-shelf.

Utility of Sunda Shelf Sediments

Though the use of shelf planktonic foraminifera to reconstruct SST and salinity may be problematic in terms of low abundance of tests, lack of appropriate temperature calibration studies, and interpretation of geochemical signals, shelf sediments are an underutilized archive. The fluvial paleochannel fill from which cores D42 and D45 were collected have preserved a thicker Holocene sedimentary package (ca. 4 m) than the adjacent shelf, which is characterized by less than 1 m of Holocene sediment (Hanebuth et al., 2002, 2011; Hanebuth and Stattegger, 2003). The two cores analyzed in this study were collected in neighboring paleochannels and are of similar length, but they provide temporal records of different length and resolution; the deeper paleochannel provided a longer temporal record n core D45, while core D42 from a shallower,

more bathymetrically subdued paleochannel resulted in higher resolution data due to the higher sedimentation rate. In addition, these sediments are generally undisturbed chronologically (excluding the 2–3.5 ka mixed section in both cores). Shelf sediments from fluvial paleochannels could be useful for studying more terrestrially influenced proxies such as bulk magnetic susceptibility, clay mineralogy, titanium abundance, or flux of organic matter.

CONCLUSIONS

Planktonic foraminiferal Mg/Ca and $\delta^{18}O_c$ data from cores D42 and D45 allow for the estimation of SST and salinity values on the Sunda Shelf for the past ~7.2 ka. Relatively low salinity estimates and $\delta^{13}C$ values in D45, as well as a simultaneous increase in sedimentation rate, suggest an increase in terrestrial runoff from ~6–4 ka, consistent with Borneo stalagmite $\delta^{18}O$ and pollen records from mainland Southeast Asia. The MCA and LIA may be recorded in the D42 and D45 SST records, but the temporal resolution and relatively high calculation-associated errors preclude a confident interpretation of these events. Nevertheless, Sunda Shelf sediments, comprising the fill of flooded fluvial paleochannels, provide a generally well-preserved record of climate change in the mid- to late Holocene.

REFERENCES

An, Z., Kukla, G., Porter, S., Xiao, J., 1991. Magnetic susceptibility evidence of monsoon variation on the loess plateau of central China during the Last 130,000 years. Quaternary Research 36, 29–36.

Anand, P., Elderfield, H., Conte, M.H., 2003. Calibration of Mg/Ca thermometry in planktonic foraminifera from a sediment trap time series. Paleoceanography 18, 1050.

Bemis, B. E., Spero, H. J., Bijima, J., Lea, D. W., 1998. Reevaluation of the oxygen isotopic composition of planktonic foraminifera: experimental results and revised paleotemperature equations. Paleoceanography 13, 150–160.

Bohaty, S.M., Zachos, J.C., Delaney, M.L., 2012. Foraminiferal Mg/Ca evidence for Southern Ocean cooling across the Eocene–Oligocene transition. Earth and Planetary Science Letters 317–318, 251–261

Boyle, E. A., 1981. Cadmium, copper, zinc, and barium in foraminiferal tests. Earth and Planetary Science Letters 53, 11–35.

Chabangborn, A. Wohlfarth, B., 2014. Climate over mainland Southeast Asia 10.5–5 ka. Journal of Quaternary Science 29, 445–454.

Cheng, X., Huang, B., Han, Z., Quanhong, Z., Tian, J., Li, J., 2005. Foraminiferal isotopic evidence for monsoonal activity in the South China Sea: a present-LGM comparison. Marine Micropaleontology 54, 125–139.

Darmadi, Y., Willis, B.J., Dorobek, S.L., 2007. Three-dimensional seismic architecture of fluvial sequences on the low-gradient Sunda Shelf, offshore Indonesia. Journal of Sedimentary Research 77, 225–238.

de Garidel-Thoron, T., Rosenthal, Y., Bassinot, F., Beaufort, L., 2005. Stable sea surface temperatures in the western Pacific warm pool over the past 1.75 million years. Nature 433, 294–298.

Dekens, P.S., Lea, D.W., Pak, D.K., Spero, H.J., 2002. Core top calibration of Mg/Ca in tropical foraminifera: refining paleotemperature estimation. Geochemistry, Geophysics, Geosystems 3, 1-29.

Ding, Y., 1994. Monsoons Over China. Kluwer Academics, Norwell, MA, 419 pp.

Dykoski, C.A., Edwards, L., Cheng, H., Yuan, D., Cai, Y., Zhang, M., Lin, Y., Qing, J., An, A., Revenaugh, J., 2005. A high-resolution, absolute-dated Holocene and deglacial Asian monsoon record from Dongge Cave, China. Earth and Planetary Science Letters 233, 71–86.

Dong, J., Wang, Y., Cheng, H., Hardt, B., Edwards, R.L., Kong, X., Wu, J., Chen, S., Liu, D., Jiang, X., Zhao, K., 2010. A high-resolution stalagmite record of the Holocene East Asian monsoon from Mt Shennongjia, central China. The Holocene 20, 257–264.

Dykoski, C. A., Edwards, R. L., Cheng, H., Yuan, D., Cai, Y., Zhang, M., Lin, Y., Qing, J., An, Z., Revenaugh, J., 2005. A high-resolution, absolute-dated Holocene and deglacial Asian monsoon record from Dongge Cave, China. Earth and Planetary Science Letters 233, 71–86.

Elderfield, H., Ganssen, G., 2000. Past temperature and $\delta^{18}O$ of surface ocean waters inferred from foraminiferal Mg/Ca ratios. Nature 405, 442–445.

Elderfield, H., Yu, J., Anand, P., Kiefer, T., Nyland, B., 2006. Calibrations for benthic foraminiferal Mg/Ca paleothermometry and the carbonate ion hypothesis. Earth and Planetary Science Letters 250, 633–649.

Fairbanks, R.G., Sverdlove, M., Free, R., Wiebe, P.H., Bé, A.W.H., 1982. Vertical distribution and isotopic fractionation of living planktonic foraminifera from the Panama Basin. Nature 298, 841–844.

Fairbanks, R.G., Wiebe, P.H., Bé, A.W.H., 1980. Vertical distribution and isotopic composition of living planktonic foraminifera in the Western North Atlantic. Science 207, 61–63.

Farmer, E.C., Kaplan, A., de Menocal, P.B., Lynch-Stieglitz, J., 2007. Corroborating ecological depth preferences of planktonic foraminifera in the tropical Atlantic with the stable oxygen isotope ratios of core top specimens. Paleoceanography 22, PA3205.

Fong, S.K., Wang, A. (Eds.), 2001. Climatological Atlas for Asian Summer Monsoon. Macau Foundation, Macau, 318 pp.

Hanebuth, T.J.J., Stattegger, K., 2003. The stratigraphic evolution of the Sunda Shelf during the past fifty thousand years. In Sidi, F.H., Nummedal, D., Inbert, P., Darman, H., Posamentier, H. (Eds.), Tropical Deltas of Southeast Asia-Sedimentology, Stratigraphy, and Petroleum Geology. SEPM Special Publication No. 76, pp. 189–200.

Hanebuth, T.J.J., Stattegger, K., Saito, Y., 2002. The stratigraphic architecture of the central Sunda Shelf (SE Asia) recorded by shallow-seismic surveying. Geo-Marine Letters 22, 86–94.

Hanebuth, T.J.J., Voris, H.K., Yokoyama, Y., Saito, Y., Okuno, J., 2011. Formation and fate of sedimentary depocentres on Southeast Asia's Sunda Shelf over the past sea-level cycle and biogeographic implications. Earth-Science Reviews 104, 92–110.

Haslett, J., Parnell, A., 2008. A simple monotone process with application to radiocarbon-dated depth chronologies. Journal of the Royal Statistical Society Series C (Applied Statistics) 57, 399–418.

Hastings, D.W., Kienast, M., Steinke, S., Whitko, A.A., 2001. A comparison of three independent paleotemperature estimates from a high resolution record of deglacial SST records in the tropical South China Sea. EOS 82, PP12B-10.

Hertzberg, J.E., Schmidt, M.W., 2013. Refining Globigerinoides ruber Mg/Ca paleothermometry in the Atlantic Ocean. Earth and Planetary Science Letters 383, 123–133.

Hönisch, B., Allen, K.A., Lea, D.W., Spero, H.J., Eggins, S.M., Arbuszewski, J., deMenocal, P., Rosenthal, Y., Russell, A.D., Elderfield, H., 2013. The influence of salinity on Mg/Ca in planktic foraminifers – evidence from cultures, core-top sediments, and complimentary $\delta^{18}O$. Geochimica et Cosmochimica Acta 121, 196–213.

Hu, C., Henderson, G.M., Huang, J., Xie, S., Sun, Y., Johnson, K.R., 2008. Quantification of Holocene Asian monsoon rainfall from spatially separated cave records. Earth and Planetary Science Letters 266, 221–232.

Huang, C., Liew, P., Zhao, M., Chang, T., Kuo, C., Chen, M., Wang, C., Zheng, L., 1997. Deep sea and lake records of the Southeast Asian paleomonsoons for the last 25 thousand years. Earth and Planetary Science Letters 146, 59–72.

Jia, G., Peng, P., Zhao, Q., Jian, Z., 2003. Changes in terrestrial ecosystem since 30 Ma in East Asia: stable isotopic evidence from black carbon in the South China Sea. Geology 31, 1093–1096.

Kienast, M., Steinke, S., Stattegger, K., Calvert, S.E., 2001. Synchronous tropical South China Sea SST change and Greenland warming during deglaciation. Science 291, 2132–2134.

Kong, D., Zong, Y. Jia, G., Wei, G., Chen, M.-T., Liu, Z., 2014. The development of late Holocene coastal cooling in the northern South China Sea. Quaternary International 349, 300–307.

Lea., D.W., Mashiotta, T.A., Spero, H.J., 1999. Controls on magnesium and strontium uptake in planktonic foraminifera determined by live culturing. Geochimica et Cosmochimica Acta 63, 2369–2379.

Lea, D.W., Pak, D.K., Spero, H.J., 2000. Climate impacts of Late Quaternary equatorial Pacific sea surface temperature variations. Science 289, 1719–1724.

Lin, H.L., Wang, W.C., Hung, G.W., 2004. Seasonal variation of planktonic foraminiferal isotopic composition from sediment traps in the South China Sea. Marine Micropaleontology 53, 447–460.

Linsley, B.K., Rosenthal, Y., Oppo, D.W., 2010. Holocene evolution of the Indonesian throughflow and the western Pacific warm pool. Nature Geoscience 3, 578–583.

Locarnini, R. A., A. V. Mishonov, J. I. Antonov, T. P. Boyer, H. E. Garcia, O. K. Baranova, M. M. Zweng, C. R. Paver, J. R. Reagan, D. R. Johnson, M. Hamilton, D. Seidov, 2013. World Ocean Atlas 2013, Volume 1: Temperature. S. Levitus, Ed., A. Mishonov Technical Ed.; NOAA Atlas NESDIS 73, 40 pp.

Maher, B.A., Thompson, R., Zhou, L.P., 1994. Spatial and temporal reconstructions of changes in the Asian paleomonsoon: A new mineral magnetic approach. Earth and Planetary Science Letters 125, 461–471.

Miao, Q., Thunell, R., Anderson, D., 1994. Glacial-Holocene carbonate dissolution and sea-surface temperatures in the South China and Sulu seas. Paleoceanography 9, 269–290.

Morimoto, M., Abe, O., Kyanne, H., Kurita, N., Matsumoto, E., Yoshida, N., 2002. Salinity records for the 1997–98 El Niño from Western Pacific corals. Geophysical Research Letters 29, 1540, 35-1–35-4.

Morse, J., Bender, M., 1990. Partition-coefficients in calcite: examination of factors influencing the validity of experimental results and their application to natural systems. Chem. Geol. 82, 265–277.

Moyer, R. P., Grottoli, A.G., 2011. Coral skeletal carbon isotopes ($\delta^{13}C$ and $\Delta^{14}C$) record the delivery of terrestrial carbon to the coastal waters of Puerto Rico. Coral Reefs 30, 791–802.

Mulitza, S., Arz, H., Kemle-von Mucke, S., Moos, C., Niebler, H.S., Patzold, J., Segl, M., 1999. The South Atlantic Carbon Isotope Record of Planktonic Foraminifera, in: Fischer, G., Wefer, G. (Eds.), Use of Proxies in Paleoceanography: Examples from the South Atlantic. Springer-Verlag, Berlin Heidelberg, pp. 427-445.

Mulitza, S., Niebler, H.S., Duerkoop, A., Wefer, G., 1997. Planktonic foraminifera as recorders of past surface water stratification. Geology 25, 335–338.

Newton, A., Thunell, R., Stott, L., 2006. Climate and hydrographic variability in the Indo-Pacific Warm Pool during the last millennium. Geophysical Research Letters 33, L19710.

Newton, A., Thunell, R., Stott, L., 2011. Changes in the Indonesian Throughflow during the past 2000 yr. Geology 39, 63–66.

Nürnberg, D., Bijma, J., Hemleben, C., 1996. Assessing the reliability of magnesium in foraminiferal calcite as a proxy for water mass temperatures. Geochimica et Cosmochimica Acta 60, 803–814.

Nürnberg, D., Müller, A., Schneider, R., 2000. Paleo-sea surface temperature calculations in the equatorial east Atlantic from Mg/Ca ratios in planktic foraminifera: A comparison to sea surface temperature estimates from Uk37, oxygen isotopes, and foraminiferal transfer functions. Paleoceanography 15, 124–134.

Partin, J.W., Cobb, K.M., Adkins, J.F., Clark, B., Fernandez, D.P., 2007. Millennial-scale trends in west Pacific warm pool hydrology since the Last Glacial Maximum. Nature 449, 452–455.

Prell, W., Kutzbach, J., 1987. Monsoon variability over the past 150,000 years. Journal of Geophysical Research-Atmospheres 92, 8411–8425.

R Development Core Team, 2011. R: a language and environment for statistical computing. 3-900051-07-0R Foundation for Statistical Computing, Vienna, Austria.

Rashid, H., England, E., Thompson, L., Polyak, L., 2011. Late Glacial to Holocene Indian Summer Monsoon variability based upon sediment records taken from the Bay of Bengal. Terr. Atmos. Ocean. Sci. 22, No. 2, 215-228.

Regenberg, M., Steph, S., Nürnberg, D., Tiedemann, R., Garbe-Schönberg, D., 2009. Calibrating Mg/Ca ratios of multiple planktonic foraminiferal species with δ^{18}O-calcification temperatures: paleothermometry for the upper water column. Earth and Planetary Science Letters 278, 324–336.

Reimer, P.J., Baillie, M.G.L., Bard., E., Bayliss, A., Beck, J.W., Blackwell, P.G., Bronk Ramsey, C., Buck, C.E., Burr, G.S., Edwards, R.L., Friedrich, M., Grootes, P.M., Guilderson, T.P., Hajdas, I., Heaton, T.J., Hogg, A.G., Hughen, K.A., Kaiser, K.F., Kromer, B., McCormac, F.G., Manning, S.W., Reimer, R.W., Richards, D.A., Southon, J.R., Talamo, S., Turney, C.S.M., van der Plicht, J., Weyhenmeyer, C.E., 2009. IntCal09 and Marine09 radiocarbon age calibration curves, 0–50,000 years cal BP. Radiocarbon 51, 1111–1150.

Reimer, P.J., Bard, E., Bayliss, A., Beck, J.W., Blackwell, P.G., Bronk, R.C., Buck, C.E., Cheng, H., Edwards, R.L., Friedrich, M., Grootes, P.M., Guilderson, T.P., Haflidason, H., Hajdas, I., Hatté, C., Heaton, T.J., Hoffmann, D.L., Hogg, A.G., Hughen, K.A., Kaiser, K.F., Kromer, B., Manning, S.W., Niu, M., Reimer, R.W., Richards, D.A., Scott, E.M., Southon, J.R., Staff, R.A., Turney, C.S.M., van der Plicht, J., 2013. IntCal13 and Marine13 radiocarbon age calibration curves 0–50,000 years cal BP. Radiocarbon 55, 1869–1887.

Rosenthal, Y., Oppo, D.W., Linsley, B.K., 2003. The amplitude and phasing of climate change during the last deglaciation in the Sulu Sea, western equatorial Pacific. Geophysical Research Letters 30, 1428.

Russell, A.D., Hönisch, B., Spero, H.J., Lea, D.W., 2004. Effects of seawater carbonate ion concentration and temperature on shell U, Mg, and Sr in cultured planktonic foraminifera. Geochimica et Cosmochimica Acta 68, 4347–4361.

Sarnthein, M., Pflaumann, U., Wang, P.X., Wong, H.K., 1994. Preliminary report on Sonne-95 Cruise "Monitor Monsoon" to the South China Sea. Kiel University, Germany , 1–225.

Schmidt, M.W., Vautravers, M.J., Spero, H.J., 2006. Rapid subtropical North Atlantic salinity oscillations across Dansgaard-Oeschger cycles. Nature 443, 561–564.

Schmidt, M.W., Lynch-Stieglitz, J., 2011. Florida Straits deglacial temperature and salinity change: implications for tropical hydrologic cycle variability during the Younger Dryas. Paleoceanography 26, PA4205.

Selvaraj, K., Wei, K.-Y., Liu, K.-K., Kao, S.-J., 2012. Late Holocene monsoon climate of north-eastern Taiwan inferred from elemental (C, N) and isotopic (δ13C, δ15N) data in lake sediments. Quaternary Science Reviews 37, 48–60.

Steinke, S., Chiu, H.-Y., Yu, P.-S., Shen, C.-C., Erlenkeuser, H., Löwemark, L., Chen, M.,-T., 2006. On the influence of sea level and monsoon climate on the southern South China Sea freshwater budget over the last 22,000 years. Quaternary Science Reviews 25, 1475–1488.

Steinke, S., Kienast, M., Pflaumann, U., Weinelt, M., Stattegger, K., 2001. A high-resolution sea-surface temperature record from the tropical South China Sea (16,500–3000 yr B.P.). Quaternary Research 55, 352–362.

Steinke, S., Mohtadi, M., Groeneveld, J., Lin, L.-C., Löwemark, L., Chen, M.-T., Rendle-Bühring, R., 2010. Reconstructing the southern South China Sea upper water column

structure since the Last Glacial Maximum: Implications for the East Asian winter monsoon development. Paleoceanography 25, PA2219.

Steinke, S., Prange, M., Feist, C., Groeneveld, J., Mohtadi, M., 2014. Upwelling variability off southern Indonesia over the past two millennia. Geophysical Research Letters 41.

Sun, M., Chiu, C.H., Shen, C.C., Lee, T., 1999. Sr thermometer for Porites corals: Little need to measure Ca? Geochemical Journal, 33, 351–354.

Thompson, P.R., 1981. Planktonic foraminifera in the Western North Pacific during the past 150,000 years: comparison of modern and fossil assemblages. Palaeogeography, Palaeoclimatology, Palaeoecology 35, 241–279.

Thunell, R.C., Miao Qingmin, Calvert, S.E., Pedersen, T.F., 1992. Glacial-Holocene biogenic sedimentation patterns in the South China Sea: productivity variations and surface water pCO_2. Paleoceanography 7, 143–162.

Wang, L., Sarnthein, M., Erlenkeuser, H., Grimalt, J., Grootes, P., Heilig, S., Ivanova, E., Kienast, M., Pelejero, C., Pflaumann, U., 1999. East Asian monsoon climate during the Late Pleistocene: high-resolution sediment records from the south China Sea. Marine Geology 156, 245–284.

Wang, L., Wang, P., 1990. Late Quaternary paleoceanography of the South China Sea: glacial-interglacial contrast in an enclosed basin. Palaeoceanography 5, 77–90.

Wang, P., Jian, Z., Liu, Z., 1992. Late Quaternary sedimentation rate in the South China Sea. In Ye, Z., Wang, P. (Eds.), Contributions to late Quaternary Paleoceanography of the South China Sea. Qingdao Ocean Press, Qingdao, pp. 22–41.

Wang, R., Abelmann, A., 2002. Radiolarian responses to paleoceanographic events of the southern South China Sea during the Pleistocene. Marine Micropaleontology 46, 25–44.

Wang, Y.J. Cheng, H., Edwards, R. L., He, Y., Kong, X., An, Z., Wu, J., Kelly, M. J., Dykoski, C. A., Li, X., , 2005. The Holocene Asian Monsoon: links to solar changes and North Atlantic climate. Science 308, 854–857.

Webster, P., Magana, V., Palmer, T., Shukla, J., Tomas, R., Yanai, M., Yasunari, T., 1998. Monsoons: processes, predictability, and the prospects for prediction. Journal of Geophysical Research-Oceans 103, 14451–14510.

Wefer, G. et al., 1999. Calculated sea surface temperatures of two sediment cores. Supplement to Wefer, G., Berger, W.H., Bijma, J., and Fischer, G., Clues to Ocean History: a brief overview of proxies. In Fischer, G. and Wefer, G. (Eds.), Use of Proxies in Paleoceanography – Examples from the South Atlantic. Springer, Berlin, Heidelberg, 1–68.

Weldeab, S., Lea, D.W., Schneider, R.R., Andersen, N., 2007. 155,000 years of West African Monsoon and ocean thermal evolution. Science 316, 1303–1307.

Wong, H.K., Ludmann, T., Haft, C., Paulson, A., Hubscher, C., Geng., J., 2003. Quaternary sedimentation in the Molengraaff paleo-delta, northern Sunda Shelf (southern South China Sea). In Sidi, F.H., Nummedal, D., Inbert, P., Darman, H., Posamentier, H. (Eds.), Tropical Deltas of Southeast Asia-Sedimentology, Stratigraphy, and Petroleum Geology. SEPM Special Publication No. 76, pp. 201–216.

Wyrtki, K., 1961. The thermohaline circulation in relation to the general circulation in the oceans. Deep-Sea Research 8, 39–64.

Xiao, J., Porter, S.C., An, Z., Kumai, H., and Yoshikawa, S., 1995. Grain size of quartz as an indicator of winter monsoon strength on the Loess Plateau of central China during the last 130,000 yr. Quaternary Research 43, 22–29.

Yoshino, M.M., 1971. Water balance problems in monsoon Asia from the viewpoint of climatology. In Yoshino, M.M. (Ed.), Water Balance of Monsoon Asia. University of Hawaii Press, Honolulu, HI, pp. 1–23.

Yu, K.F., Zhao, J.X., Wei, G.J. Chang, X.R., and Wang, P.X., 2005. Mid-late Holocene monsoon climate retrieved from seasonal Sr/Ca and delta O-18 records of *Porites lutea* corals at Leizhou Peninsula, northern coast of South China Sea. Global and Planetary Change 47, 301–316.

Zhang, P.Z., Cheng, H., Edwards, R.L., et al., 2008. A test of climate, sun, and culture relationships from an 1810-year Chinese cave record. Science 322, 940–942.

Zhao, C., Chang, Y.-P., Chen, M.-T., and Liu, Z., 2013. Possible reverse trend in Asian summer monsoon strength during the late Holocene. Journal of Asian Earth Science 69, 102–112.

Zweng, M.M, J.R. Reagan, J.I. Antonov, R.A. Locarnini, A.V. Mishonov, T.P. Boyer, H.E. Garcia, O.K. Baranova, D.R. Johnson, D.Seidov, M.M. Biddle, 2013. World Ocean Atlas 2013, Volume 2: Salinity. S. Levitus, Ed., A. Mishonov Technical Ed.; NOAA Atlas

NESDIS 74, 39 pp.

APPENDIX A

Core logs

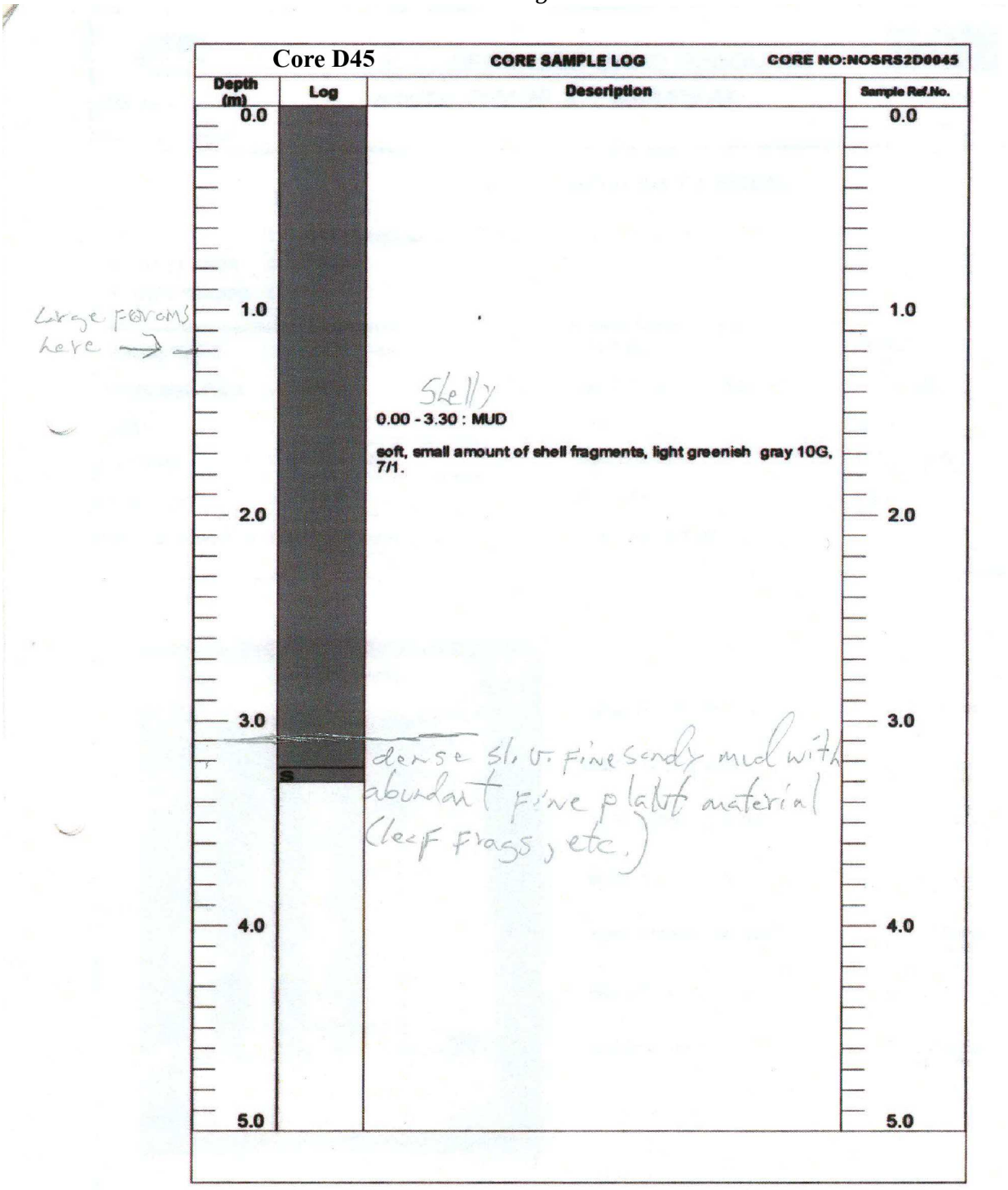

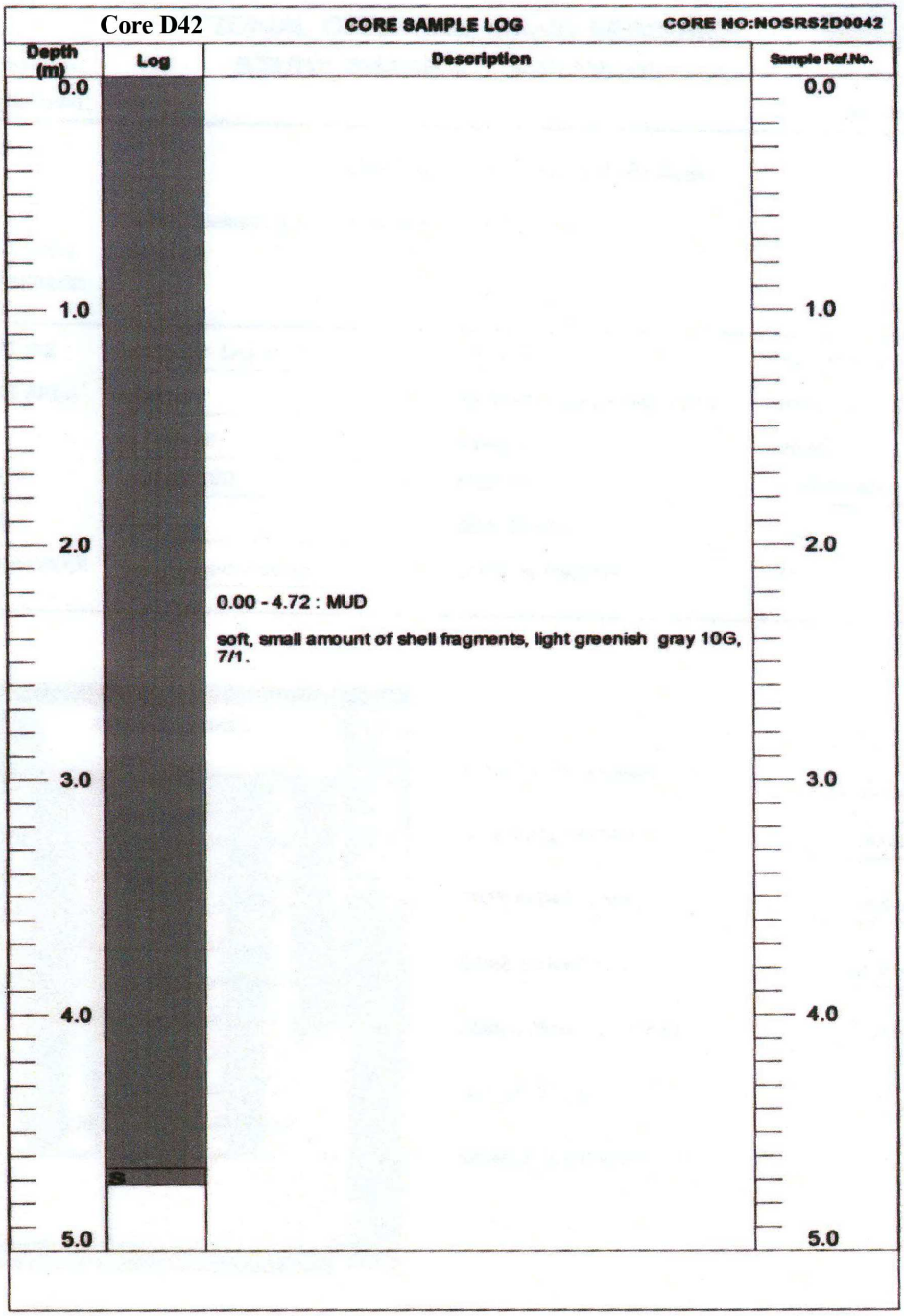
Core D42
CORE SAMPLE LOG
CORE NO:NOSRS2D0042
Depth (m)
Log
Description
Sample Ref.No.
0.0
1.0
2.0
3.0
4.0
5.0
0.00 - 4.72 : MUD
soft, small amount of shell fragments, light greenish gray 10G, 7/1.
S

APPENDIX B

Mg/Ca Cleaning Procedure for Foraminifera
Modified from the Marine Sediment Research Laboratory, University of South Carolina

Chemical Preparation

1. *Oxidizing Reagent (0.15% H_2O_2 in 0.1 N NaOH)*

Prepare by mixing 50 mL of 0.1N NaOH with 2.5 mL of 3% H_2O_2 (or 0.25 mL 30% H_2O_2).

2. *Weak Acid Leach Solution (0.001M HNO_3)*

Prepare by mixing 200 µL of 1M HNO_3 with 200 ml of MQ-H_2O.

Cleaning Protocol

STEP 1: Pre-Clean, Weigh, and Crush Samples

1. Using methanol to pick, load enough pre-cleaned foraminiferal specimens into a copper boat to equal ~250 µg on the microbalance. Methanol will evaporate quickly so wait for mass to balance.
2. Record weight and number of foraminifera.
3. Transfer weighed foraminifera into 1.5 mL centrifuge tube with labeled cap.
4. Working with underlight microscope and gloves, add 200 µL of methanol to each centrifuge tube.
5. Hold tube between fingers and use 1000 µL pipette and tips (set at ~ 700 µL) to "pop" foraminifera (pop open but do not pulverize) against side of tube.
6. Pipette off as much supernatant as possible without disturbing foraminifera.
7. Repeat with separate pipette tip for each sample.

STEP 2: Clay Removal

1. Add 100 µL of pure H_2O to each tube to just cover samples. Tap the tray on the lab bench to get rid of air bubbles and knock down fragments.
2. Sonicate tray for one minute.
3. Under microscope, working one row of samples at a time, disturb each sample with 400 µL of pure water to help suspend clays.
4. Under microscope, tap vial to knock down fragments and siphon off the supernatant. Repeat. Use separate pipette tips for each sample.
5. Repeat steps (1-4) twice.
6. Using gloves, add 400 µL of methanol to each tube.
7. Sonicate tray for 1 minute.

8. Siphon off supernatant.
9. Repeat steps (6-8) once.
10. Rinse tubes with 400 µL of pure water.
11. Sonicate tray for 1 minute.
12. Siphon off supernatant.
13. Rinse tubes again with 400 µL of pure water.
14. Siphon off supernatant.

STEP 4: Removal of Organic Matter with Oxidizing Agent

1. Add 250 µL oxidizing reagent to each tube.
2. Cap tubes and place in boiling water bath for 10 minutes.
    a. During this time, label a new set of clean, acid-washed tubes.
3. Tap on bench to knock down material from sides and eliminating bubbles.
4. Siphon, removing oxidizing agent
5. Add 400 µL of pure water to each tube.
6. Sonicate for 1 minute.
7. Siphon off water.
8. Add 400 µL pure water and siphon.

Transfer Samples to New Vials

1. Using new set of pipette tips, add 100-150 µL of ultrapure water to each tube.
2. Switching tips between samples, transfer samples to new, acid washed tubes.
3. Add 200 µL of ultrapure water to old tube. Transfer water and foraminiferal fragments into new tube with a pipette. Repeat twice for a total of three rinses.
4. Siphon off all water.

STEP 5: Weak Acid Leach

1. Working one row at a time, add 250 µL of 0.001M HNO_3.
2. Sonicate for 30 seconds.
3. Add 400 µL of pure water. Rap rack firmly on bench.
4. Siphon off supernatant using individual pipette tips for each sample.
5. Add 400 µL of pure water.
6. Remove all supernatant.

STEP 6: Dissolution

1. Add enough 5% HNO_3 to each sample to yield a Ca concentration of 80 ppm.
2. Cap and sonicate samples for 1 minute.

Calculation: Amount of acid to add (in mL) = [(sample weight (µg)/2)*0.4]/80

APPENDIX C

Radiocarbon age estimates calibrated using the Marine09 dataset

	Age (cal kyr BP)		
Sample ID	**2.50%**	**50%**	**97.50%**
D45_10-12	0.509	0.562	0.625
D45_16-18	0.65	0.692	0.754
D45_24-26	0.549	0.62	0.667
D45_34-36	1.095	1.189	1.252
D45_48-50	1.4	1.484	1.567
D45_60-62	1.587	1.69	1.791
D45_74-76	1.832	1.908	1.985
D45_98-100	2.161	2.26	2.319
D45_112-114	3.308	3.391	3.488
D45_122-124	4.085	4.203	4.342
D45_132-134	4.404	4.478	4.581
D45_148-150	4.517	4.627	4.768
D45_162-164	4.802	4.855	4.951
D45_182-184	5.038	5.168	5.27
D45_198-200	5.312	5.392	5.501
D45_214-216	5.478	5.581	5.67
D45_232-234	6.315	6.397	6.474
D45_248-250	7.154	7.22	7.292
D42_8-10	0.659	0.708	0.78
D42_24-26	1.324	1.395	1.489
D42_56-58	1.383	1.461	1.537
D42_110-112	1.932	2.018	2.107
D42_198-200	3.275	3.372	3.459
D42_276-278	3.134	3.242	3.328
D42_356-358	3.159	3.256	3.331

APPENDIX D

Modeled age-depth data for D45

D45	Age (cal kyr BP)			D45 (cont.)	Age (cal kyr BP)		
Depth (cm)	2.50%	50%	97.50%	Depth (cm)	2.50%	50%	97.50%
1	0.013	0.037	0.257	40	1.214	1.280	1.390
2	0.030	0.086	0.340	41	1.222	1.299	1.399
3	0.046	0.134	0.381	42	1.230	1.317	1.409
4	0.063	0.183	0.412	43	1.239	1.336	1.418
5	0.080	0.231	0.435	44	1.249	1.355	1.430
6	0.100	0.280	0.455	45	1.261	1.373	1.446
7	0.125	0.328	0.473	46	1.277	1.392	1.464
8	0.155	0.377	0.491	47	1.300	1.410	1.482
9	0.189	0.425	0.512	48	1.346	1.429	1.501
10	0.245	0.474	0.543	49	1.420	1.448	1.542
11	0.385	0.522	0.589	50	1.443	1.469	1.583
12	0.540	0.555	0.616	51	1.453	1.489	1.607
13	0.554	0.575	0.633	52	1.462	1.509	1.622
14	0.564	0.595	0.646	53	1.470	1.529	1.634
15	0.575	0.616	0.662	54	1.478	1.550	1.645
16	0.588	0.636	0.684	55	1.487	1.570	1.655
17	0.619	0.656	0.712	56	1.496	1.590	1.665
18	0.647	0.676	0.749	57	1.507	1.610	1.676
19	0.651	0.695	0.778	58	1.520	1.631	1.690
20	0.655	0.715	0.802	59	1.537	1.651	1.710
21	0.658	0.734	0.830	60	1.567	1.671	1.731
22	0.661	0.754	0.859	61	1.628	1.691	1.757
23	0.665	0.773	0.887	62	1.649	1.706	1.797
24	0.669	0.793	0.918	63	1.667	1.720	1.819
25	0.678	0.812	0.953	64	1.683	1.734	1.834
26	0.718	0.842	1.021	65	1.697	1.749	1.845
27	0.761	0.880	1.060	66	1.706	1.763	1.853
28	0.801	0.918	1.086	67	1.713	1.777	1.861
29	0.840	0.957	1.106	68	1.720	1.791	1.868
30	0.865	0.995	1.122	69	1.728	1.806	1.875
31	0.888	1.033	1.138	70	1.735	1.820	1.882
32	0.909	1.072	1.153	71	1.744	1.834	1.893
33	0.944	1.110	1.168	72	1.756	1.849	1.908
34	0.993	1.148	1.191	73	1.769	1.863	1.924
35	1.117	1.187	1.229	74	1.792	1.877	1.941
36	1.155	1.206	1.312	75	1.849	1.892	1.965
37	1.176	1.224	1.346	76	1.882	1.907	2.040
38	1.194	1.243	1.365	77	1.896	1.922	2.088
39	1.203	1.262	1.380	78	1.902	1.938	2.116

D45 (cont.)	Age (cal kyr BP)			D45 (cont.)	Age (cal kyr BP)		
Depth (cm)	2.50%	50%	97.50%	Depth (cm)	2.50%	50%	97.50%
79	1.907	1.953	2.137	122	3.779	4.140	4.218
80	1.911	1.968	2.153	123	4.024	4.225	4.258
81	1.916	1.984	2.164	124	4.143	4.270	4.340
82	1.921	1.999	2.174	125	4.177	4.290	4.371
83	1.926	2.015	2.182	126	4.207	4.310	4.388
84	1.931	2.030	2.190	127	4.234	4.329	4.400
85	1.936	2.045	2.198	128	4.260	4.349	4.409
86	1.941	2.061	2.204	129	4.282	4.369	4.420
87	1.947	2.076	2.210	130	4.298	4.388	4.434
88	1.953	2.091	2.216	131	4.318	4.408	4.459
89	1.958	2.107	2.222	132	4.352	4.428	4.486
90	1.966	2.122	2.228	133	4.415	4.441	4.517
91	1.974	2.138	2.233	134	4.433	4.448	4.536
92	1.982	2.153	2.238	135	4.441	4.454	4.551
93	1.991	2.168	2.243	136	4.444	4.461	4.562
94	2.002	2.184	2.249	137	4.446	4.468	4.574
95	2.014	2.199	2.256	138	4.449	4.474	4.584
96	2.031	2.214	2.266	139	4.452	4.481	4.595
97	2.053	2.230	2.278	140	4.454	4.487	4.606
98	2.094	2.245	2.291	141	4.457	4.494	4.618
99	2.182	2.261	2.325	142	4.461	4.501	4.628
100	2.273	2.324	2.735	143	4.464	4.507	4.640
101	2.307	2.405	2.919	144	4.468	4.514	4.652
102	2.335	2.486	3.006	145	4.473	4.520	4.664
103	2.363	2.566	3.062	146	4.480	4.527	4.675
104	2.390	2.647	3.113	147	4.489	4.534	4.689
105	2.419	2.728	3.153	148	4.509	4.540	4.703
106	2.450	2.809	3.189	149	4.547	4.553	4.730
107	2.479	2.889	3.221	150	4.555	4.574	4.756
108	2.512	2.970	3.249	151	4.563	4.595	4.770
109	2.555	3.051	3.278	152	4.570	4.616	4.781
110	2.603	3.132	3.307	153	4.578	4.637	4.790
111	2.684	3.212	3.337	154	4.586	4.658	4.800
112	2.830	3.293	3.379	155	4.594	4.679	4.809
113	3.283	3.374	3.460	156	4.603	4.700	4.817
114	3.403	3.459	3.805	157	4.613	4.721	4.825
115	3.437	3.544	3.926	158	4.625	4.742	4.836
116	3.470	3.629	3.993	159	4.637	4.763	4.849
117	3.502	3.714	4.043	160	4.651	4.784	4.864
118	3.536	3.799	4.081	161	4.675	4.805	4.878
119	3.573	3.885	4.118	162	4.721	4.826	4.894
120	3.618	3.970	4.150	163	4.820	4.846	4.931
121	3.686	4.055	4.183	164	4.837	4.865	5.005

D45 (cont.)	Age (cal kyr BP)			D45 (cont.)	Age (cal kyr BP)		
Depth (cm)	2.50%	50%	97.50%	Depth (cm)	2.50%	50%	97.50%
165	4.850	4.884	5.049	208	5.444	5.529	5.568
166	4.857	4.903	5.076	209	5.454	5.536	5.572
167	4.863	4.923	5.095	210	5.466	5.543	5.581
168	4.869	4.942	5.112	211	5.475	5.550	5.592
169	4.875	4.961	5.124	212	5.483	5.557	5.605
170	4.881	4.980	5.135	213	5.494	5.564	5.616
171	4.887	4.999	5.144	214	5.509	5.571	5.630
172	4.893	5.018	5.153	215	5.547	5.584	5.690
173	4.900	5.037	5.160	216	5.587	5.630	5.952
174	4.908	5.056	5.167	217	5.603	5.676	6.065
175	4.916	5.075	5.174	218	5.619	5.721	6.124
176	4.924	5.094	5.180	219	5.634	5.767	6.159
177	4.933	5.113	5.186	220	5.649	5.813	6.188
178	4.944	5.132	5.192	221	5.664	5.858	6.218
179	4.958	5.151	5.198	222	5.679	5.904	6.242
180	4.979	5.170	5.205	223	5.695	5.950	6.261
181	5.006	5.189	5.211	224	5.713	5.995	6.279
182	5.041	5.208	5.218	225	5.730	6.041	6.295
183	5.077	5.225	5.281	226	5.750	6.087	6.311
184	5.099	5.240	5.338	227	5.772	6.133	6.325
185	5.116	5.256	5.363	228	5.799	6.178	6.339
186	5.133	5.271	5.379	229	5.827	6.224	6.354
187	5.150	5.286	5.392	230	5.869	6.270	6.368
188	5.164	5.301	5.401	231	5.927	6.315	6.383
189	5.179	5.316	5.408	232	6.036	6.361	6.403
190	5.193	5.332	5.415	233	6.335	6.407	6.467
191	5.208	5.347	5.421	234	6.392	6.457	6.759
192	5.221	5.362	5.427	235	6.427	6.507	6.874
193	5.232	5.377	5.433	236	6.446	6.557	6.932
194	5.245	5.393	5.438	237	6.464	6.607	6.975
195	5.257	5.408	5.444	238	6.480	6.657	7.004
196	5.269	5.423	5.449	239	6.496	6.707	7.033
197	5.285	5.438	5.454	240	6.513	6.757	7.056
198	5.306	5.454	5.459	241	6.533	6.807	7.077
199	5.328	5.465	5.494	242	6.552	6.857	7.097
200	5.347	5.472	5.523	243	6.578	6.907	7.115
201	5.362	5.479	5.536	244	6.605	6.958	7.133
202	5.375	5.486	5.542	245	6.637	7.008	7.149
203	5.387	5.493	5.548	246	6.679	7.058	7.167
204	5.401	5.501	5.552	247	6.738	7.108	7.184
205	5.413	5.508	5.557	248	6.847	7.158	7.211
206	5.423	5.515	5.560	249	7.150	7.208	7.263
207	5.433	5.522	5.564	250	7.183	7.229	7.520

APPENDIX E

Modeled age-depth data for D42

D42	Age (cal kyr BP)			D42 (cont.)	Age (cal kyr BP)		
Depth (cm)	2.50%	50%	97.50%	Depth (cm)	2.50%	50%	97.50%
0	-0.002	0.015	0.037	39	1.342	1.412	1.499
1	0.045	0.089	0.197	40	1.346	1.421	1.503
2	0.100	0.164	0.328	41	1.349	1.429	1.507
3	0.147	0.238	0.410	42	1.354	1.438	1.511
4	0.197	0.313	0.464	43	1.358	1.447	1.515
5	0.248	0.387	0.517	44	1.363	1.455	1.519
6	0.315	0.462	0.564	45	1.366	1.464	1.523
7	0.393	0.536	0.617	46	1.371	1.472	1.526
8	0.520	0.611	0.678	47	1.376	1.481	1.530
9	0.651	0.685	0.751	48	1.380	1.490	1.534
10	0.707	0.728	0.834	49	1.385	1.498	1.537
11	0.731	0.766	0.935	50	1.391	1.507	1.541
12	0.751	0.803	1.007	51	1.397	1.516	1.545
13	0.771	0.840	1.052	52	1.404	1.524	1.548
14	0.790	0.878	1.086	53	1.410	1.533	1.552
15	0.809	0.915	1.113	54	1.420	1.541	1.555
16	0.829	0.952	1.137	55	1.427	1.550	1.559
17	0.850	0.989	1.157	56	1.437	1.559	1.562
18	0.870	1.027	1.176	57	1.446	1.567	1.585
19	0.895	1.064	1.194	58	1.456	1.574	1.651
20	0.924	1.101	1.219	59	1.468	1.581	1.698
21	0.954	1.139	1.249	60	1.477	1.588	1.731
22	0.988	1.176	1.285	61	1.486	1.595	1.757
23	1.044	1.213	1.325	62	1.494	1.602	1.773
24	1.141	1.250	1.365	63	1.503	1.609	1.782
25	1.276	1.288	1.403	64	1.511	1.616	1.795
26	1.296	1.300	1.417	65	1.520	1.623	1.803
27	1.299	1.309	1.427	66	1.528	1.631	1.813
28	1.303	1.317	1.437	67	1.535	1.638	1.818
29	1.306	1.326	1.445	68	1.544	1.645	1.823
30	1.310	1.334	1.453	69	1.552	1.652	1.828
31	1.314	1.343	1.459	70	1.559	1.659	1.834
32	1.317	1.352	1.466	71	1.565	1.666	1.840
33	1.321	1.360	1.471	72	1.570	1.673	1.844
34	1.324	1.369	1.475	73	1.577	1.680	1.851
35	1.328	1.378	1.480	74	1.583	1.687	1.856
36	1.331	1.386	1.485	75	1.587	1.694	1.861
37	1.335	1.395	1.491	76	1.592	1.701	1.864
38	1.339	1.403	1.495	77	1.595	1.708	1.867

D42 (cont.)	Age (cal kyr BP)		
Depth (cm)	2.50%	50%	97.50%
78	1.598	1.715	1.871
79	1.601	1.723	1.875
80	1.605	1.730	1.878
81	1.608	1.737	1.882
82	1.611	1.744	1.886
83	1.614	1.751	1.889
84	1.617	1.758	1.893
85	1.620	1.765	1.895
86	1.624	1.772	1.899
87	1.627	1.779	1.901
88	1.631	1.786	1.905
89	1.634	1.793	1.907
90	1.638	1.800	1.910
91	1.642	1.807	1.914
92	1.647	1.815	1.917
93	1.651	1.822	1.921
94	1.656	1.829	1.924
95	1.660	1.836	1.930
96	1.666	1.843	1.935
97	1.671	1.850	1.942
98	1.678	1.857	1.952
99	1.683	1.864	1.960
100	1.690	1.871	1.969
101	1.696	1.878	1.978
102	1.704	1.885	1.987
103	1.715	1.892	1.997
104	1.726	1.899	2.007
105	1.736	1.907	2.017
106	1.751	1.914	2.027
107	1.770	1.921	2.036
108	1.792	1.928	2.046
109	1.824	1.935	2.056
110	1.874	1.942	2.068
111	1.945	1.949	2.082
112	1.951	1.955	2.116
113	1.953	1.961	2.154
114	1.954	1.967	2.187
115	1.956	1.974	2.224
116	1.958	1.980	2.253
117	1.960	1.986	2.273
118	1.962	1.992	2.288
119	1.963	1.998	2.302
120	1.965	2.004	2.316

D42 (cont.)	Age (cal kyr BP)		
Depth (cm)	2.50%	50%	97.50%
121	1.967	2.010	2.331
122	1.969	2.016	2.344
123	1.971	2.022	2.362
124	1.972	2.028	2.375
125	1.974	2.034	2.391
126	1.976	2.040	2.407
127	1.978	2.046	2.419
128	1.979	2.051	2.433
129	1.981	2.057	2.450
130	1.983	2.063	2.466
131	1.985	2.069	2.479
132	1.987	2.075	2.492
133	1.989	2.080	2.502
134	1.990	2.086	2.514
135	1.992	2.091	2.527
136	1.994	2.097	2.538
137	1.996	2.102	2.548
138	1.998	2.108	2.562
139	1.999	2.114	2.576
140	2.001	2.119	2.588
141	2.003	2.124	2.599
142	2.005	2.130	2.609
143	2.007	2.135	2.619
144	2.009	2.140	2.630
145	2.011	2.145	2.639
146	2.013	2.151	2.650
147	2.015	2.157	2.661
148	2.017	2.163	2.669
149	2.019	2.168	2.679
150	2.021	2.174	2.690
151	2.024	2.180	2.699
152	2.026	2.186	2.709
153	2.028	2.192	2.719
154	2.030	2.197	2.729
155	2.032	2.203	2.739
156	2.035	2.209	2.750
157	2.037	2.215	2.760
158	2.040	2.220	2.769
159	2.043	2.226	2.779
160	2.045	2.232	2.788
161	2.048	2.238	2.798
162	2.051	2.244	2.808
163	2.054	2.249	2.818

D42 (cont.)	Age (cal kyr BP)			D42 (cont.)	Age (cal kyr BP)		
Depth (cm)	2.50%	50%	97.50%	Depth (cm)	2.50%	50%	97.50%
164	2.057	2.255	2.829	207	2.483	2.539	3.205
165	2.060	2.261	2.838	208	2.487	2.549	3.207
166	2.063	2.267	2.850	209	2.490	2.560	3.207
167	2.067	2.272	2.859	210	2.493	2.570	3.208
168	2.070	2.278	2.868	211	2.497	2.581	3.209
169	2.073	2.284	2.877	212	2.500	2.591	3.209
170	2.076	2.290	2.887	213	2.504	2.601	3.210
171	2.079	2.296	2.895	214	2.507	2.612	3.211
172	2.083	2.301	2.906	215	2.511	2.622	3.211
173	2.088	2.307	2.915	216	2.514	2.632	3.212
174	2.093	2.313	2.924	217	2.517	2.643	3.212
175	2.097	2.319	2.934	218	2.520	2.653	3.213
176	2.101	2.324	2.943	219	2.524	2.663	3.213
177	2.104	2.330	2.952	220	2.527	2.674	3.214
178	2.109	2.336	2.961	221	2.530	2.684	3.215
179	2.114	2.342	2.971	222	2.534	2.694	3.216
180	2.119	2.347	2.981	223	2.537	2.705	3.216
181	2.124	2.353	2.994	224	2.540	2.715	3.217
182	2.130	2.359	3.004	225	2.544	2.725	3.218
183	2.135	2.365	3.013	226	2.547	2.736	3.219
184	2.141	2.371	3.023	227	2.551	2.746	3.219
185	2.147	2.376	3.034	228	2.554	2.756	3.220
186	2.154	2.382	3.044	229	2.558	2.767	3.221
187	2.163	2.388	3.054	230	2.561	2.777	3.221
188	2.170	2.394	3.064	231	2.565	2.787	3.222
189	2.178	2.399	3.074	232	2.569	2.798	3.223
190	2.187	2.405	3.084	233	2.572	2.808	3.224
191	2.198	2.411	3.095	234	2.576	2.818	3.224
192	2.210	2.417	3.105	235	2.580	2.829	3.225
193	2.223	2.423	3.116	236	2.584	2.839	3.226
194	2.238	2.428	3.128	237	2.588	2.849	3.227
195	2.261	2.434	3.138	238	2.592	2.860	3.227
196	2.289	2.440	3.151	239	2.597	2.870	3.228
197	2.328	2.446	3.165	240	2.600	2.880	3.228
198	2.378	2.451	3.178	241	2.605	2.891	3.229
199	2.445	2.457	3.192	242	2.609	2.901	3.230
200	2.461	2.467	3.194	243	2.614	2.912	3.231
201	2.464	2.477	3.196	244	2.620	2.922	3.232
202	2.467	2.487	3.197	245	2.626	2.932	3.232
203	2.470	2.498	3.199	246	2.631	2.943	3.233
204	2.473	2.508	3.201	247	2.635	2.953	3.234
205	2.477	2.518	3.202	248	2.641	2.963	3.235
206	2.480	2.529	3.204	249	2.645	2.974	3.236

D42 (cont.)	Age (cal kyr BP)		
Depth (cm)	2.50%	50%	97.50%
250	2.651	2.984	3.236
251	2.656	2.994	3.237
252	2.661	3.005	3.238
253	2.668	3.015	3.238
254	2.676	3.025	3.239
255	2.682	3.036	3.240
256	2.692	3.046	3.241
257	2.697	3.056	3.242
258	2.703	3.067	3.242
259	2.710	3.077	3.243
260	2.719	3.087	3.244
261	2.729	3.098	3.245
262	2.740	3.108	3.246
263	2.751	3.118	3.247
264	2.758	3.129	3.248
265	2.768	3.139	3.249
266	2.782	3.149	3.250
267	2.794	3.160	3.251
268	2.811	3.170	3.253
269	2.823	3.180	3.254
270	2.842	3.191	3.255
271	2.864	3.201	3.256
272	2.897	3.211	3.257
273	2.939	3.222	3.258
274	2.983	3.232	3.259
275	3.053	3.242	3.261
276	3.101	3.253	3.263
277	3.150	3.262	3.269
278	3.153	3.263	3.283
279	3.156	3.264	3.290
280	3.158	3.265	3.293
281	3.159	3.266	3.296
282	3.160	3.267	3.299
283	3.162	3.268	3.301
284	3.163	3.269	3.302
285	3.165	3.269	3.304
286	3.166	3.270	3.305
287	3.167	3.271	3.306
288	3.168	3.272	3.307
289	3.170	3.273	3.308
290	3.172	3.274	3.309
291	3.174	3.275	3.310
292	3.175	3.276	3.311

D42 (cont.)	Age (cal kyr BP)		
Depth (cm)	2.50%	50%	97.50%
293	3.176	3.277	3.312
294	3.178	3.278	3.313
295	3.179	3.279	3.314
296	3.181	3.280	3.314
297	3.182	3.281	3.315
298	3.184	3.281	3.316
299	3.185	3.282	3.317
300	3.187	3.283	3.317
301	3.189	3.284	3.318
302	3.190	3.285	3.318
303	3.191	3.286	3.319
304	3.192	3.287	3.319
305	3.193	3.288	3.320
306	3.195	3.289	3.320
307	3.196	3.290	3.321
308	3.197	3.291	3.321
309	3.199	3.292	3.321
310	3.200	3.293	3.322
311	3.201	3.293	3.322
312	3.202	3.294	3.323
313	3.203	3.295	3.323
314	3.204	3.296	3.323
315	3.205	3.297	3.324
316	3.206	3.298	3.324
317	3.207	3.299	3.324
318	3.209	3.300	3.325
319	3.210	3.301	3.325
320	3.211	3.302	3.325
321	3.212	3.303	3.326
322	3.214	3.304	3.326
323	3.215	3.305	3.326
324	3.216	3.306	3.327
325	3.218	3.306	3.327
326	3.219	3.307	3.327
327	3.221	3.308	3.328
328	3.221	3.309	3.328
329	3.222	3.310	3.328
330	3.224	3.311	3.329
331	3.225	3.312	3.329
332	3.226	3.313	3.329
333	3.227	3.314	3.329
334	3.228	3.315	3.330
335	3.229	3.316	3.330

D42 (cont.)		Age (cal kyr BP)	
Depth (cm)	**2.50%**	**50%**	**97.50%**
336	3.230	3.317	3.330
337	3.231	3.318	3.331
338	3.232	3.318	3.331
339	3.234	3.319	3.331
340	3.235	3.320	3.332
341	3.236	3.321	3.332
342	3.237	3.322	3.332
343	3.238	3.323	3.332
344	3.239	3.324	3.333
345	3.241	3.325	3.333
346	3.242	3.326	3.333
347	3.243	3.327	3.334
348	3.245	3.328	3.334
349	3.246	3.329	3.334
350	3.248	3.330	3.334
351	3.249	3.330	3.335
352	3.251	3.331	3.335
353	3.252	3.332	3.335
354	3.253	3.333	3.335
355	3.254	3.334	3.336
356	3.256	3.335	3.336
357	3.259	3.337	3.390
358	3.267	3.347	3.676
359	3.272	3.357	3.862
360	3.276	3.367	4.006

APPENDIX F

Raw Mg/Ca, $\delta^{18}O_c$, $\delta^{13}C$, and % mud for D45. Values in bold were interpolated.

Mid-depth (cm)	Mg/Ca (mmol/mol)	$\delta^{18}O_c$ (‰)	$\delta^{13}C$ (‰)	% Mud
1	8.564	-3.415	0.910	98.48
3	8.930	-3.266	1.068	98.43
5	4.896	-3.718	1.065	98.16
7	6.529	-3.267	0.855	98.54
9	6.414	-3.893	0.820	97.39
11	6.627	-3.439	0.983	97.54
13	7.278	-3.144	0.813	96.51
15	6.257	-3.218	0.879	97.12
17	7.813	-3.661	0.641	93.08
19	5.781	-3.242	0.818	98.39
21	6.687	-3.327	0.787	99.07
23	6.298	-2.701	0.943	98.45
25	5.318	-3.974	0.918	97.28
27	7.960	-2.764	0.677	98.20
29	6.788	-3.569	1.006	98.88
31	5.774	-3.922	1.108	98.87
33	6.381	-3.618	0.591	98.81
35	10.790	-3.630	0.399	97.67
37	6.801	-3.418	0.698	97.93
39	10.708	-3.259	0.696	98.34
41	5.018	-3.780	0.805	96.80
43	5.153	-3.738	0.739	98.44
45	6.596	-3.587	1.044	98.01
47	5.214	-3.887	0.454	97.63
49	6.496	-3.039	1.017	96.60
51	6.027	-3.667	0.914	92.89
53	5.670	-3.229	1.201	98.79
55	5.859	-3.939	1.018	97.94
57	4.846	-3.677	0.682	98.21
59	5.278	-3.597	0.446	98.58
61	5.357	-3.543	0.911	97.98
63	4.825	-3.474	0.758	98.61
65	4.837	-3.632	0.913	98.26
67	5.392	-3.432	1.140	98.73
69	4.937	-3.300	1.113	99.05
71	4.842	-3.465	0.783	98.85
73		-3.807	0.845	99.25
75	5.548	-3.455	0.390	98.84
77	6.561	-3.606	0.606	98.64
79	6.758	-2.895	0.645	98.08
81	5.314	**-2.940**	**0.673**	99.02

Mid-depth (cm)	Mg/Ca (mmol/mol)	$\delta^{18}O_c$ (‰)	$\delta^{13}C$ (‰)	% Mud
83	5.327	**-2.984**	**0.701**	99.15
85	6.616	**-3.029**	**0.729**	99.38
87	5.195	-3.073	0.757	99.01
89	7.813	-3.464	0.366	98.80
91	5.437	-3.045	1.340	98.05
93	14.078	-3.377	0.379	96.13
95	7.220	-3.572	0.618	99.13
97	5.358	-3.446	0.338	99.14
99	6.020	-3.398	0.216	99.15
101	4.737	-3.230	0.648	99.00
103	6.869	-3.592	0.807	97.56
105	5.957	-3.619	0.787	94.59
107	5.191	-3.574	0.967	79.68
109	5.309	-3.732	1.264	94.03
111	6.647	-3.316	1.083	95.28
113	5.295	-3.345	0.322	96.38
115	4.853	-3.708	1.062	97.79
117	5.788	-3.663	0.670	97.54
119	5.710	-3.393	0.915	97.01
121	5.299	-3.636	1.080	93.52
123	5.028	-3.220	1.153	93.69
125	5.509	-3.361	0.939	98.15
127	6.274	-3.627	1.050	98.42
129	6.671	-3.047	0.631	98.41
131	5.051	-3.606	0.773	98.38
133	5.481	-3.272	0.297	97.18
135	6.643	-3.685	0.872	97.60
137	6.630	-3.805	0.518	97.60
139	4.909	-3.662	1.099	98.00
141	4.516	-3.577	1.069	98.41
143	4.974	-3.847	0.925	98.22
145	6.343	-3.696	0.588	98.60
147	4.271	-3.689	0.972	98.00
149	5.640	-3.679	0.639	98.39
151	4.914	-3.391	0.578	98.43
153	5.005	-3.916	1.189	98.17
155	4.515	-4.049	0.533	96.34
157	4.964	-3.573	0.288	97.88
159	5.225	-3.736	0.918	97.64
161	4.163	-3.109	0.370	97.15
163	4.413	-3.428	0.723	96.60
165	4.120	-3.659	0.747	98.07
167	4.634	-3.965	1.084	97.66
169	4.748	-3.628	0.733	98.29
171	4.848	-3.192	0.941	97.72

Mid-depth (cm)	Mg/Ca (mmol/mol)	$\delta^{18}O_c$ (‰)	$\delta^{13}C$ (‰)	% Mud
173	5.158	-3.328	0.470	97.51
175	4.645	-3.380	0.845	97.93
177	5.209	-3.427	1.315	98.47
179	4.949	-3.897	1.348	97.74
181	4.307	-3.803	0.881	97.41
183	5.698	-3.792	1.044	95.82
185	5.182	-3.641	1.026	92.72
187	4.817	-3.326	1.050	93.79
189	4.850	-3.101	1.150	92.94
191	6.059	-3.364	1.204	96.66
193	4.675	-3.499	0.842	97.41
195	5.226	-3.231	1.105	97.41
197	5.133	-3.491	0.912	97.51
199	5.626	-3.764	1.174	96.68
201	4.946	-3.833	1.443	96.47
203	4.264	-3.174	1.375	96.12
205	5.787	-3.251	0.890	97.13
207	5.152	-3.466	1.095	96.12
209	4.484	-3.497	1.015	96.25
211	5.293	-3.350	0.920	96.36
213	5.333	-3.762	1.043	95.10
215	5.110	-3.652	1.356	94.39
217	5.100	**-3.665**	**1.062**	95.61
219	7.465	-3.677	0.768	91.06
221	5.862	-3.684	1.049	95.80
223	5.297	-3.515	1.327	94.72
225	5.566	-3.420	1.046	91.23
227	7.274	-3.619	1.324	93.58
229	5.692	-3.519	1.362	89.89
231	6.493	-3.581	1.417	88.48
233	6.915	-3.360	1.112	88.37
235	5.601	-4.116	1.374	88.43
237	5.122	-3.776	1.077	87.78
239	5.747	-3.702	0.796	86.83
241	8.398	-3.616	1.630	81.51
243	4.459	-3.768	1.196	87.41
245	5.472	-3.603	0.962	85.23
247	4.687	-3.815	1.233	92.29
249	5.574	-3.875	0.842	89.97

APPENDIX G

Raw Mg/Ca, $\delta^{18}O_c$, $\delta^{13}C$, and % mud for D42. Values in bold were interpolated.

Mid-depth (cm)	Mg/Ca (mmol/mol)	$\delta^{18}O_c$ (‰)	$\delta^{13}C$ (‰)	% Mud
1	7.342	-3.661	0.692	97.20
3	5.958	-3.692	0.770	96.99
5	8.588	-3.571	0.949	97.01
7	7.480	-3.421	0.707	97.95
9	6.223	-3.620	0.908	97.98
11		-3.518	1.150	97.13
13	5.262	-3.513	1.022	96.97
15	5.647	-3.379	0.908	97.40
17	7.633	-3.717	0.861	97.62
19	5.781	-3.381	0.578	95.96
21	4.519	-3.674	0.992	96.86
23	5.261	-3.644	0.929	97.28
25	9.017	-3.585	1.359	97.59
27	6.423	-3.357	0.534	97.93
29	5.772	-3.183	0.606	98.62
31	4.952	-3.462	0.561	98.52
33	7.748	-3.476	0.862	98.54
35	4.662	-3.268	0.560	98.10
37	7.377	-3.476	1.227	95.53
39	5.328	-3.536	1.072	97.40
41		-3.366	0.518	97.41
43	4.765	**-3.459**	**0.759**	98.08
45	5.842	-3.552	1.000	97.72
47	5.551	-3.745	1.542	97.59
49	4.415	-3.662	0.923	97.67
51	5.123	-3.330	0.953	97.52
53	5.091	-2.953	1.110	97.53
55	5.302	-3.459	0.924	97.47
57	7.120	-3.277	1.067	98.53
59	5.383	-3.678	1.103	97.79
61	5.273	-3.781	1.290	98.15
63	5.245	-3.579	0.703	98.23
65	5.094	-3.375	1.274	98.51
67	4.886	-3.348	1.228	98.74
69	4.848	-3.554	0.986	98.58
71	5.507	-3.630	1.005	98.56
73	4.984	-3.673	0.744	98.80
75	6.355	-3.646	0.975	98.66
77	5.169	-3.455	0.850	98.73
79		**-3.563**	**0.910**	98.45
81	6.658	-3.672	0.971	98.64

Mid-depth (cm)	Mg/Ca (mmol/mol)	$\delta^{18}O_c$ (‰)	$\delta^{13}C$ (‰)	% Mud
83	6.953	-3.694	1.091	98.11
85	5.148	-3.482	1.228	97.78
87	4.736	-3.534	1.060	98.29
89	5.242	-3.540	0.677	98.14
91	4.837	-3.312	0.988	98.46
93	5.576	-3.590	0.925	98.69
95	6.459	-3.679	0.940	98.21
97	6.698	-3.554	1.050	98.44
99	5.388	-3.775	0.874	98.87
101	4.294	-3.296	0.665	97.74
103	7.138	-3.299	1.113	98.59
105	6.134	-3.600	0.977	98.13
107	4.636	-3.682	1.027	98.53
109	5.232	**-3.778**	**1.226**	98.18
111	6.109	-3.874	1.424	98.24
113	5.228	-3.281	0.962	98.36
115	4.409	-3.497	0.990	98.06
117		-3.750	0.790	98.03
119	5.133	-3.956	1.088	97.68
121	5.448	-3.685	1.089	98.70
123	5.211	-3.387	1.066	98.49
125	4.881	-3.295	1.095	97.90
127	4.562	-3.393	0.921	98.42
129	6.235	-3.888	1.113	98.70
131		-3.460	0.740	98.44
133	5.105	-3.222	0.671	98.26
135	5.545	-3.688	0.705	97.95
137	4.988	-3.576	0.942	97.61
139	4.781	-3.715	1.111	97.85
141	4.444	-3.796	0.890	98.36
143	6.025	-3.639	0.880	98.16
145	5.397	-3.596	0.707	97.67
147	6.008	-3.323	0.792	98.12
149	6.136	-3.545	0.971	96.89

APPENDIX H

Calculated SST, $\delta^{18}O_{sw}$, and salinity for D45. Values in bold were interpolated.

Mid-depth (cm)	SST (°C)	$\delta^{18}O_{sw}$	Salinity
1	32.40	0.232	34.60
3	32.77	0.458	35.14
5	27.46	-1.102	31.42
7	30.00	-0.120	33.76
9	29.85	-0.779	32.19
11	30.14	-0.265	33.42
13	30.96	0.202	34.53
15	29.63	-0.150	33.69
17	31.59	-0.184	33.61
19	28.93	-0.320	33.29
21	30.21	-0.136	33.72
23	29.68	0.379	34.95
25	28.19	-1.205	31.18
27	31.76	0.748	35.83
29	30.35	-0.351	33.21
31	28.92	-1.002	31.66
33	29.80	-0.513	32.83
35	34.45	0.443	35.10
37	30.36	-0.196	33.58
39	34.38	0.800	35.95
41	27.67	-1.119	31.38
43	27.91	-1.028	31.60
45	30.09	-0.422	33.04
47	28.01	-1.155	31.30
49	29.96	0.098	34.28
51	29.30	-0.667	32.46
53	28.75	-0.343	33.23
55	29.05	-0.992	31.69
57	27.36	-1.080	31.48
59	28.12	-0.843	32.04
61	28.25	-0.761	32.24
63	27.33	-0.885	31.94
65	27.35	-1.039	31.57
67	28.31	-0.638	32.53
69	27.53	-0.668	32.46
71	27.36	-0.869	31.98
73	**27.96**	**-1.086**	**31.46**
75	28.56	-0.609	32.60
77	30.05	-0.450	32.98
79	30.31	0.315	34.80
81	28.18	**-0.173**	**33.64**
83	28.20	**-0.213**	**33.54**
85	30.12	**0.142**	**34.39**
87	27.98	-0.348	33.22
89	31.59	0.013	34.08
91	28.38	-0.236	33.49
93	**29.64**	**-0.306**	**33.32**
95	30.89	-0.241	33.47
97	28.25	-0.664	32.47
99	29.28	-0.401	33.09
101	27.16	-0.676	32.44
103	30.45	-0.352	33.21
105	29.19	-0.642	32.52
107	27.97	-0.850	32.02
109	28.17	-0.967	31.75
111	30.16	-0.137	33.72
113	28.15	-0.584	32.66
115	27.38	-1.108	31.41
117	28.94	-0.739	32.29
119	28.82	-0.493	32.87
121	28.16	-0.874	31.97
123	27.69	-0.555	32.73
125	28.50	-0.528	32.79
127	29.65	-0.554	32.73
129	30.19	0.139	34.38
131	27.73	-0.933	31.83
133	28.46	-0.448	32.98
135	30.16	-0.507	32.84
137	30.14	-0.630	32.55
139	27.48	-1.041	31.57
141	26.74	-1.111	31.40
143	27.60	-1.202	31.19
145	29.75	-0.603	32.61
147	26.25	-1.325	30.89

Mid-depth (cm)	SST (°C)	$\delta^{18}O_{sw}$	Salinity
149	28.71	-0.802	32.14
151	27.49	-0.768	32.22
153	27.65	-1.260	31.05
155	26.74	-1.582	30.28
157	27.58	-0.932	31.83
159	28.03	-1.000	31.67
161	26.02	-0.793	32.16
163	26.54	-1.003	31.66
165	25.93	-1.361	30.81
167	26.97	-1.451	30.59
169	27.18	-1.068	31.50
171	27.37	-0.595	32.63
173	27.92	-0.616	32.58
175	26.99	-0.861	32.00
177	28.00	-0.697	32.39
179	27.55	-1.261	31.04
181	26.32	-1.423	30.66
183	28.80	-0.896	31.91
185	27.96	-0.920	31.86
187	27.31	-0.740	32.29
189	27.37	-0.503	32.85
191	29.34	-0.356	33.20
193	27.05	-0.969	31.74
195	28.03	-0.494	32.87
197	27.87	-0.788	32.17
199	28.69	-0.892	31.92
201	27.55	-1.199	31.19
203	26.23	-0.813	32.11
205	28.94	-0.327	33.27
207	27.91	-0.756	32.25
209	26.68	-1.043	31.56
211	28.15	-0.590	32.64
213	28.21	-0.989	31.69
215	27.84	-0.957	31.77
217	27.82	**-0.973**	**31.73**
219	31.19	-0.284	33.37
221	29.05	-0.736	32.30
223	28.15	-0.754	32.25
225	28.59	-0.568	32.70
227	30.96	-0.274	33.40
229	28.79	-0.626	32.56
231	29.95	-0.445	32.99
233	30.51	-0.108	33.79
235	28.65	-1.252	31.07
237	27.86	-1.077	31.48
239	28.87	-0.791	32.16
241	32.23	-0.006	34.03
243	26.63	-1.325	30.89
245	28.44	-0.782	32.19
247	27.07	-1.279	31.00
249	28.60	-1.020	31.62

APPENDIX I

Calculated SST, $\delta^{18}O_{sw}$, and salinity for D42. Values in bold were interpolated.

Mid-depth (cm)	SST (°C)	$\delta^{18}O_{sw}$	Salinity	Mid-depth (cm)	SST (°C)	$\delta^{18}O_{sw}$	Salinity
1	31.04	-0.299	33.34	77	27.94	-0.739	32.29
3	29.19	-0.714	32.35	79	**29.06**	**-0.614**	**32.59**
5	32.43	0.081	34.24	81	30.18	-0.489	32.88
7	31.21	-0.023	33.99	83	30.56	-0.431	33.02
9	29.58	-0.561	32.71	85	27.90	-0.774	32.21
11	**28.81**	**-0.620**	**32.57**	87	27.16	-0.979	31.72
13	28.09	-0.764	32.23	89	28.06	-0.798	32.15
15	28.72	-0.499	32.86	91	27.35	-0.719	32.34
17	31.39	-0.282	33.38	93	28.61	-0.734	32.30
19	28.93	-0.459	32.96	95	29.91	-0.553	32.73
21	26.75	-1.206	31.18	97	30.23	-0.360	33.19
23	28.09	-0.896	31.91	99	28.30	-0.983	31.71
25	32.86	0.157	34.42	101	26.29	-0.922	31.85
27	29.86	-0.240	33.48	103	30.79	0.012	34.08
29	28.91	-0.263	33.42	105	29.45	-0.568	32.69
31	27.56	-0.826	32.08	107	26.97	-1.166	31.27
33	31.52	-0.014	34.01	109	28.04	**-1.040**	**31.57**
35	27.02	-0.742	32.28	111	29.41	-0.850	32.02
37	31.08	-0.104	33.80	113	28.04	-0.544	32.75
39	28.20	-0.764	32.23	115	26.53	-1.075	31.49
41	**27.71**	**-0.697**	**32.39**	117	**27.20**	**-1.187**	**31.22**
43	27.22	**-0.893**	**31.92**	119	27.88	-1.252	31.07
45	29.02	-0.610	32.60	121	28.40	-0.872	31.97
47	28.57	-0.898	31.91	123	28.01	-0.656	32.49
49	26.54	-1.237	31.10	125	27.43	-0.685	32.42
51	27.86	-0.631	32.55	127	26.83	-0.908	31.89
53	27.80	-0.265	33.42	129	29.60	-0.826	32.08
55	28.16	-0.696	32.39	131	**28.69**	**-0.586**	**32.65**
57	30.77	0.029	34.12	133	27.83	-0.530	32.79
59	28.30	-0.887	31.93	135	28.56	-0.843	32.04
61	28.11	-1.028	31.60	137	27.62	-0.926	31.84
63	28.07	-0.836	32.06	139	27.25	-1.143	31.33
65	27.81	-0.686	32.41	141	26.60	-1.359	30.81
67	27.44	-0.736	32.30	143	29.29	-0.641	32.52
69	27.37	-0.956	31.77	145	28.32	-0.801	32.14
71	28.50	-0.798	32.15	147	29.27	-0.330	33.26
73	27.61	-1.024	31.61	149	29.45	-0.513	32.83
75	29.76	-0.549	32.74				

APPENDIX J

Five-point smoothed SST, $\delta^{18}O_c$, salinity, and $\delta^{13}C$ for D45

Mid-depth (cm)	SST (°C)	$\delta^{18}O_c$ (‰)	Salinity	$\delta^{13}C$ (‰)
5	30.50	-3.51	33.42	0.94
7	30.04	-3.52	33.19	0.96
9	29.68	-3.49	33.07	0.91
11	30.12	-3.39	33.52	0.87
13	30.43	-3.47	33.49	0.83
15	30.25	-3.34	33.71	0.83
17	30.26	-3.32	33.77	0.79
19	30.01	-3.23	33.85	0.81
21	29.72	-3.38	33.35	0.82
23	29.75	-3.20	33.79	0.83
25	30.04	-3.27	33.78	0.87
27	29.78	-3.39	33.37	0.93
29	29.80	-3.57	32.94	0.86
31	31.05	-3.50	33.73	0.76
33	30.78	-3.63	33.28	0.76
35	31.58	-3.57	33.82	0.70
37	31.33	-3.54	33.77	0.64
39	30.96	-3.57	33.52	0.67
41	30.08	-3.56	33.11	0.80
43	29.61	-3.65	32.66	0.75
45	28.73	-3.61	32.32	0.81
47	29.05	-3.58	32.54	0.83
49	29.22	-3.48	32.86	0.93
51	29.01	-3.55	32.59	0.92
53	28.88	-3.51	32.63	0.97
55	28.52	-3.62	32.18	0.85
57	28.31	-3.60	32.13	0.85
59	28.02	-3.65	31.88	0.76
61	27.68	-3.58	31.85	0.74
63	27.87	-3.54	32.06	0.83
65	27.75	-3.48	32.15	0.97
67	27.57	-3.46	32.10	0.94
69	27.70	-3.53	32.00	0.96
71	27.94	-3.49	32.20	0.85
73	28.29	-3.53	32.29	0.75
75	28.85	-3.45	32.76	0.65
77	29.01	-3.34	33.09	0.63
79	29.06	-3.18	33.51	0.60
81	29.37	-3.09	33.87	0.67
83	28.96	-2.98	33.92	0.70
85	29.22	-3.10	33.77	0.65

Mid-depth (cm)	SST (°C)	$\delta^{18}O_c$ (‰)	Salinity	$\delta^{13}C$ (‰)
87	29.26	-3.12	33.74	0.78
89	29.54	-3.20	33.70	0.71
91	29.70	-3.31	33.52	0.69
93	29.75	-3.38	33.36	0.61
95	29.29	-3.37	33.17	0.58
97	29.05	-3.40	32.96	0.44
99	29.21	-3.45	32.94	0.53
101	28.87	-3.46	32.75	0.56
103	28.81	-3.48	32.66	0.68
105	28.59	-3.55	32.39	0.89
107	29.19	-3.57	32.64	0.98
109	28.73	-3.52	32.53	0.88
111	28.37	-3.53	32.31	0.94
113	28.56	-3.55	32.36	0.88
115	28.69	-3.48	32.59	0.81
117	28.29	-3.55	32.24	0.81
119	28.20	-3.52	32.25	0.98
121	28.42	-3.45	32.53	0.95
123	28.56	-3.45	32.62	1.03
125	28.84	-3.38	32.92	0.97
127	28.75	-3.37	32.89	0.91
129	28.91	-3.38	32.94	0.74
131	29.24	-3.45	32.95	0.72
133	29.34	-3.48	32.91	0.62
135	28.79	-3.61	32.35	0.71
137	28.59	-3.60	32.27	0.77
139	28.42	-3.72	31.91	0.90
141	28.34	-3.72	31.86	0.84
143	27.56	-3.69	31.53	0.93
145	27.81	-3.70	31.65	0.84
147	27.96	-3.66	31.81	0.74
149	27.97	-3.67	31.78	0.79
151	27.37	-3.74	31.32	0.78
153	27.63	-3.72	31.50	0.65
155	27.50	-3.73	31.41	0.70
157	27.20	-3.68	31.40	0.66
159	26.98	-3.58	31.52	0.57
161	26.82	-3.50	31.62	0.61
163	26.70	-3.58	31.38	0.77
165	26.53	-3.56	31.34	0.73
167	26.80	-3.57	31.44	0.85
169	27.07	-3.55	31.62	0.79
171	27.29	-3.50	31.86	0.81
173	27.49	-3.39	32.22	0.86
175	27.57	-3.44	32.13	0.98

Mid-depth (cm)	SST (°C)	$\delta^{18}O_c$ (‰)	Salinity	$\delta^{13}C$ (‰)
177	27.36	-3.57	31.73	0.97
179	27.53	-3.66	31.60	1.09
181	27.73	-3.71	31.57	1.12
183	27.59	-3.69	31.55	1.07
185	27.55	-3.53	31.91	1.03
187	28.16	-3.44	32.42	1.09
189	27.81	-3.39	32.39	1.05
191	27.82	-3.30	32.59	1.07
193	27.93	-3.34	32.57	1.04
195	28.20	-3.47	32.38	1.05
197	27.84	-3.56	31.98	1.10
199	27.67	-3.50	32.05	1.20
201	27.86	-3.50	32.13	1.16
203	27.86	-3.50	32.15	1.20
205	27.46	-3.44	32.08	1.16
207	27.58	-3.35	32.37	1.06
209	27.98	-3.47	32.28	0.99
211	27.76	-3.55	31.98	1.09
213	27.74	-3.59	31.88	1.08
215	28.64	-3.62	32.24	1.03
217	28.82	-3.69	32.17	1.06
219	28.81	-3.64	32.28	1.11
221	28.96	-3.59	32.47	1.05
223	29.59	-3.58	32.80	1.10
225	29.11	-3.55	32.64	1.22
227	29.29	-3.53	32.78	1.30
229	29.76	-3.50	33.09	1.25
231	29.77	-3.64	32.76	1.32
233	29.15	-3.67	32.38	1.27
235	29.17	-3.71	32.30	1.16
237	29.62	-3.71	32.51	1.20
239	28.85	-3.80	31.93	1.21
241	28.81	-3.69	32.15	1.13
243	28.65	-3.70	32.06	1.16
245	28.60	-3.74	31.95	1.17

APPENDIX K

Five-point smoothed SST, $\delta^{18}O_c$, salinity, and $\delta^{13}C$ for D42

Mid-depth (cm)	SST (°C)	$\delta^{18}O_c$ (‰)	Salinity	$\delta^{13}C$ (‰)
5	30.69	-3.59	33.33	0.81
7	30.24	-3.56	33.17	0.90
9	30.02	-3.53	33.15	0.95
11	29.28	-3.49	32.87	0.94
13	29.32	-3.55	32.75	0.97
15	29.19	-3.50	32.80	0.90
17	28.77	-3.53	32.52	0.87
19	28.77	-3.56	32.46	0.85
21	29.60	-3.60	32.77	0.94
23	29.30	-3.53	32.79	0.88
25	29.29	-3.49	32.88	0.88
27	29.46	-3.45	33.06	0.80
29	30.14	-3.41	33.48	0.78
31	28.97	-3.35	33.05	0.62
33	29.22	-3.37	33.12	0.76
35	29.08	-3.44	32.88	0.86
37	29.11	-3.42	32.94	0.85
39	28.25	-3.42	32.52	0.83
41	28.65	-3.48	32.59	0.92
43	28.14	-3.53	32.21	0.98
45	27.81	-3.56	31.98	0.95
47	27.84	-3.55	32.02	1.04
49	27.96	-3.45	32.31	1.11
51	27.79	-3.43	32.27	1.09
53	28.23	-3.34	32.71	1.00
55	28.58	-3.34	32.88	1.03
57	28.63	-3.43	32.69	1.10
59	28.68	-3.55	32.42	1.02
61	28.61	-3.54	32.42	1.09
63	27.94	-3.55	32.06	1.12
65	27.76	-3.53	32.03	1.10
67	27.84	-3.50	32.14	1.04
69	27.74	-3.52	32.05	1.05
71	28.14	-3.57	32.11	0.99
73	28.24	-3.59	32.11	0.91
75	28.57	-3.59	32.27	0.90
77	28.91	-3.60	32.42	0.89
79	29.50	-3.61	32.70	0.96
81	29.13	-3.57	32.60	1.01
83	28.97	-3.59	32.48	1.05
85	28.77	-3.58	32.39	1.01

Mid-depth (cm)	SST (°C)	$\delta^{18}O_c$ (‰)	Salinity	$\delta^{13}C$ (‰)
87	28.21	-3.51	32.29	1.01
89	27.82	-3.49	32.14	0.98
91	28.22	-3.53	32.25	0.92
93	28.83	-3.53	32.54	0.92
95	28.88	-3.58	32.45	0.96
97	28.67	-3.58	32.36	0.89
99	29.11	-3.52	32.71	0.93
101	29.01	-3.50	32.70	0.94
103	28.36	-3.53	32.32	0.93
105	28.31	-3.53	32.29	1.00
107	28.93	-3.65	32.33	1.15
109	28.38	-3.64	32.06	1.12
111	27.80	-3.62	31.82	1.13
113	27.85	-3.64	31.81	1.08
115	27.81	-3.67	31.71	1.05
117	27.61	-3.63	31.70	0.98
119	27.60	-3.65	31.65	1.00
121	27.78	-3.61	31.83	1.03
123	27.71	-3.54	31.97	1.05
125	28.05	-3.53	32.17	1.06
127	28.11	-3.48	32.30	0.99
129	28.08	-3.45	32.36	0.91
131	28.30	-3.53	32.29	0.83
133	28.46	-3.57	32.28	0.83
135	27.99	-3.53	32.13	0.83
137	27.57	-3.60	31.76	0.86
139	27.86	-3.68	31.71	0.91
141	27.82	-3.66	31.73	0.91
143	28.14	-3.61	32.01	0.88
145	28.59	-3.58	32.31	0.85